

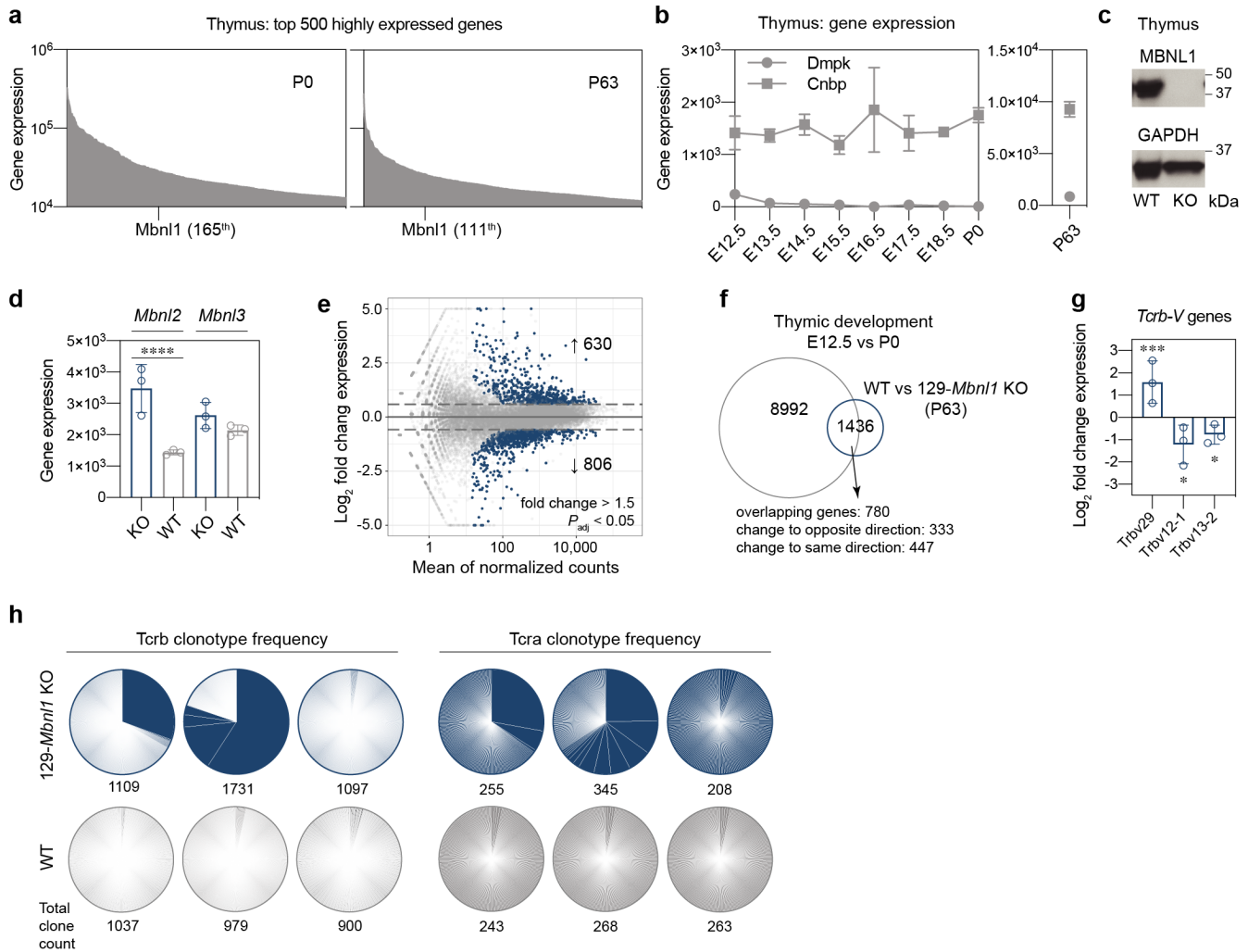
Supplementary Information

Loss of MBNL1 induces RNA mis-processing  
in the thymus and peripheral blood

Ł. J. Sznajder et al.

## Table of Contents

Supplementary Figure 1. Gene expression changes in 129- <i>Mbnl1</i> KO thymus	p. 3-4
Supplementary Figure 2. Thymic pathology in 129- <i>Mbnl1</i> KO	p. 5-6
Supplementary Figure 3. Genome browser views of selected mouse alternative splicing events	p. 7-12
Supplementary Figure 4. MBNL1 directly regulates Lef1 E6	p. 13-14
Supplementary Figure 5. Alternative splicing changes in <i>Mbnl1</i> KO splenocytes and PBMCs	p. 15
Supplementary Figure 6. Alternative splicing changes in DM2 PBMCs	p. 16-17
Supplementary Figure 7. Gene expression changes in DM2 whole blood	p. 18
Supplementary Figure 8. Genome browser views of selected human alternative splicing events	p. 19-31
Supplementary Figure 9. Alternative splicing changes in DM2 whole blood	p. 32-33
Supplementary Figure 10. Blood DM2 alternative splicing changes are not age dependent	p. 34
Supplementary Figure 11. Graphical abstract	p. 35
Supplementary References	p. 36



### Supplementary Fig. 1. Gene expression changes in 129-*Mbn1* KO thymus

**a** Top 500 highly expressed genes in postnatal day 0 (P0;  $n = 2$ ) and 63 (P63;  $n = 3$ ) thymus RNA-seq data. *Mbn1* is the 165<sup>th</sup> and 111<sup>th</sup> highest expressed gene at P0 and P63, respectively. P0 RNA-seq data were obtained from GSE107910<sup>1</sup> and P63 represents our RNA-seq.

**b** *Dmpk* and *Cnbp* gene expression levels during thymus organogenesis and in the postnatal gland. RNA-seq was performed at embryonic (E) days: 12.5 ( $n = 3$ ), 13.5 ( $n = 3$ ), 14.5 ( $n = 2$ ), 15.5 ( $n = 2$ ), 16.5 ( $n = 3$ ), 17.5 ( $n = 2$ ), 18.5 ( $n = 2$ ) and postnatal day 0 (P0;  $n = 2$ ) and 63 (P63;  $n = 3$ ). Data from embryonic and P0 thymi were obtained from GSE107910<sup>1</sup> and P63 represents our RNA-seq. Points connected by lines show mean expression  $\pm$  standard deviation (SD).

**c** MBNL1 protein is not detectable in *Mbn1* knockout (KO) thymus by western blot. WT - wild type. Uncropped and unprocessed scans of the blots containing molecular weight markers are provided in the Source Data file.

**d** *Mbn2* gene expression increases in *Mbn1* KO ( $n = 3$ ) compared to WT ( $n = 3$ ) thymus. *Mbn3* expression level is unchanged. Bar graph shows mean expression  $\pm$  SD. DESeq2; \*\*\*\* adjusted  $P$  value ( $P_{adj}$ )  $< 0.0001$ .

**e** Differential gene expression analysis for 129-*Mbn1* KO. Blue dots on the volcano plot represent differentially expressed genes in *Mbn1* KO thymus RNA-seq.

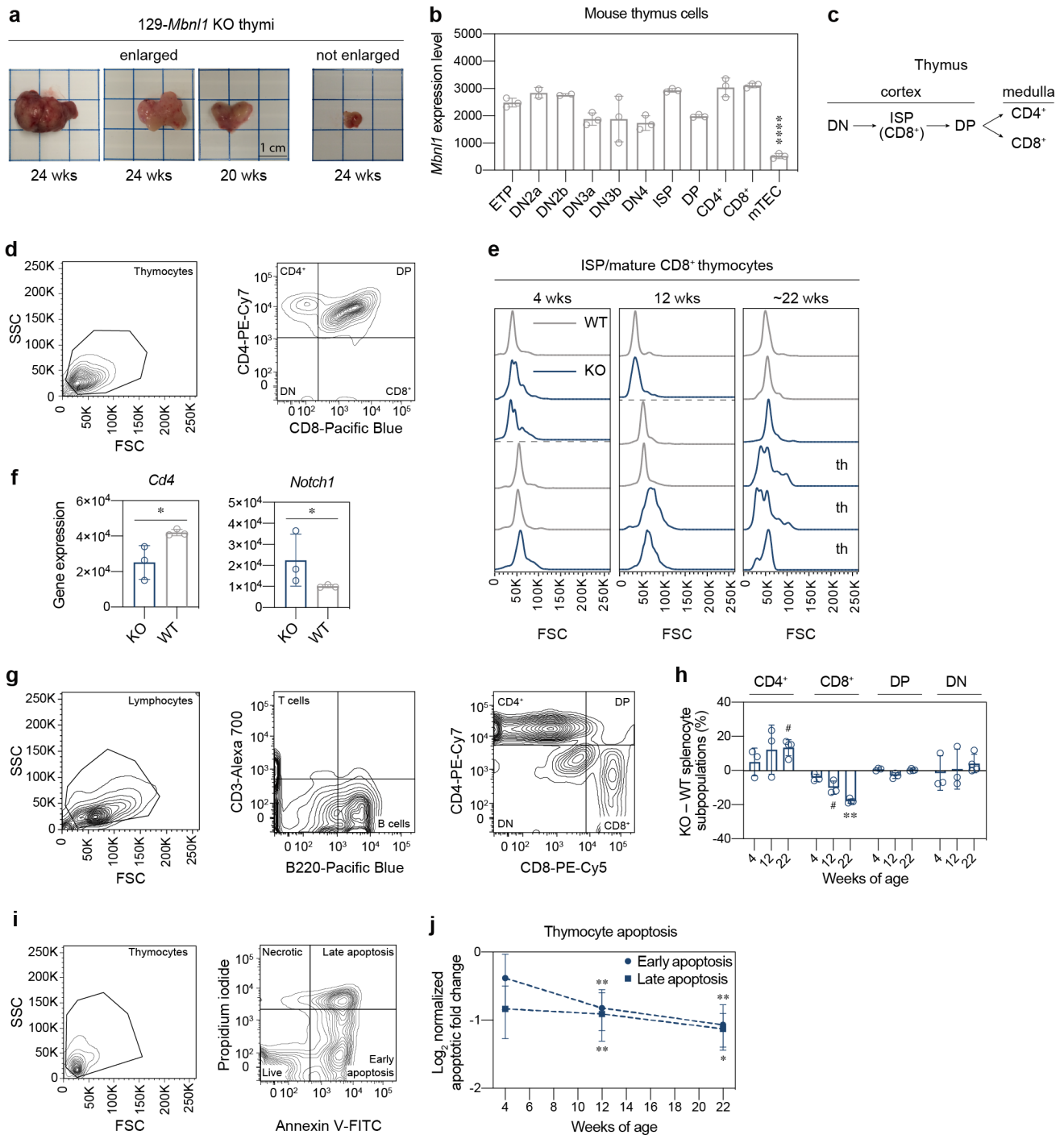
**f** Venn diagram shows differentially expressed genes during embryonic thymus organogenesis (embryonic day (E)12.5 vs P0) and at postnatal day 63 thymus with depleted Mbn1 protein (WT vs 129-*Mbn1* KO). Data from embryonic and P0 thymi were obtained from GSE107910<sup>1</sup> and P63 represents our RNA-seq.

**g** TCR beta variable genes mis-expression in 129-*Mbn1* KO (n = 3) compared to WT (n = 3) thymus RNA-seq. Bar graph shows mean  $\pm$  SD. DESeq2; \*  $P_{adj} < 0.05$ , \*\*\*  $P_{adj} = 0.0005$ .

**h** Pie charts represent Tcrb and Tcra clonotype frequencies in 129-*Mbn1* KO (n =3) and WT (n = 3) thymic RNA-seq.

Source data are provided as the Source Data and Supplementary Data 1 files.





## Supplementary Fig. 2. Thymic pathology in 129-*Mbn1* KO

**a** Photos of enlarged/not enlarged thymi in 129-*Mbn1* KO at 20-24 weeks of age (wks).

**b** *Mbn1* expression in mouse Early T lineage Precursor (ETP; CD4<sup>-</sup>, CD8<sup>-</sup>, CD11b<sup>-</sup>, CD11c<sup>-</sup>, CD19<sup>-</sup>, NK1.1<sup>-</sup>, TCR<sup>-</sup>, CD44<sup>hi</sup>, CD117<sup>hi</sup>, CD25<sup>-</sup>), Double Negative 2a (DN2a; CD4<sup>-</sup>, CD8<sup>-</sup>, CD11b<sup>-</sup>, CD11c<sup>-</sup>, CD19<sup>-</sup>, NK1.1<sup>-</sup>, TCR<sup>-</sup>, CD44<sup>hi</sup>, CD117<sup>hi</sup>, CD25<sup>hi</sup>), Double Negative 2b (DN2b; CD4<sup>-</sup>, CD8<sup>-</sup>, CD11b<sup>-</sup>, CD11c<sup>-</sup>, CD19<sup>-</sup>, NK1.1<sup>-</sup>, TCR<sup>-</sup>, CD44<sup>hi</sup>, CD117<sup>int</sup>, CD25<sup>hi</sup>), Double Negative 3a (DN3a; CD4<sup>-</sup>, CD8<sup>-</sup>, CD11b<sup>-</sup>, CD11c<sup>-</sup>, CD19<sup>-</sup>, NK1.1<sup>-</sup>, TCR<sup>-</sup>, CD44<sup>-</sup>, CD25<sup>hi</sup>, CD28<sup>-</sup>), Double-Negative 3b (DN3b; CD4<sup>-</sup>, CD8<sup>-</sup>, CD11b<sup>-</sup>, CD11c<sup>-</sup>, CD19<sup>-</sup>, NK1.1<sup>-</sup>, TCR<sup>-</sup>, CD44<sup>-</sup>, CD25<sup>hi</sup>, CD28<sup>+</sup>), Double Negative 4 (DN4; CD4<sup>-</sup>, CD8<sup>-</sup>, CD11b<sup>-</sup>, CD11c<sup>-</sup>, CD19<sup>-</sup>, NK1.1<sup>-</sup>, TCR<sup>-</sup>, CD44<sup>-</sup>, CD25<sup>-</sup>, CD28<sup>+</sup>), Immature Single Positive (ISP; CD4<sup>-</sup>, CD8<sup>+</sup>, TCR<sup>-/lo</sup>, CD24<sup>hi</sup>), Double Positive (DP; CD4<sup>+</sup>, CD8<sup>+</sup>, TCR<sup>-/lo</sup>, CD69<sup>-</sup>), Mature CD4 Single

Positive (CD4<sup>+</sup>; CD4<sup>+</sup>, CD8<sup>-</sup>, TCR<sup>hi</sup>, CD24<sup>-/lo</sup>), Mature CD8 Single Positive (CD8<sup>+</sup>; CD4<sup>-</sup>, CD8<sup>+</sup>, TCR<sup>hi</sup>, CD24<sup>-/lo</sup>), and Medullary Thymic Epithelial Cells (mTEC; CD45<sup>-</sup>, EpCAM<sup>+</sup>, Ly51<sup>-</sup>, MHCII<sup>hi</sup>). Gene expression obtained from the BloodSpot database (servers.binf.ku.dk/bloodspot)<sup>2</sup>; Dataset: Mouse ImmGen Microarray - GSE15907 (Immunological Genome Project; www.immgen.org). Bar graph shows mean expression  $\pm$  SD. Significant difference was determined by Dunnett's multiple comparisons test. \*\*\*\*  $P_{adj} < 0.0001$ .

**c** Mouse thymocyte development scheme.

**d** Schematic of gating strategy for the flow cytometry analysis of thymocyte subpopulations.

**e** Flow cytometry Forward Scatter (FSC) parameter plots showing different relative thymocyte CD8<sup>+</sup> cell sizes in 129-*Mbn1* KO (th - thymus hyperplasia).

**f** *Cd4* and *Notch1* gene expression decrease and increases in *Mbn1* KO (n = 3) compared to WT (n = 3) thymus, respectively. Bar graphs show mean expression  $\pm$  SD. DESeq2; \*  $P_{adj} < 0.05$ .

**g** Schematic of gating strategy for the flow cytometry analysis of splenocytes.

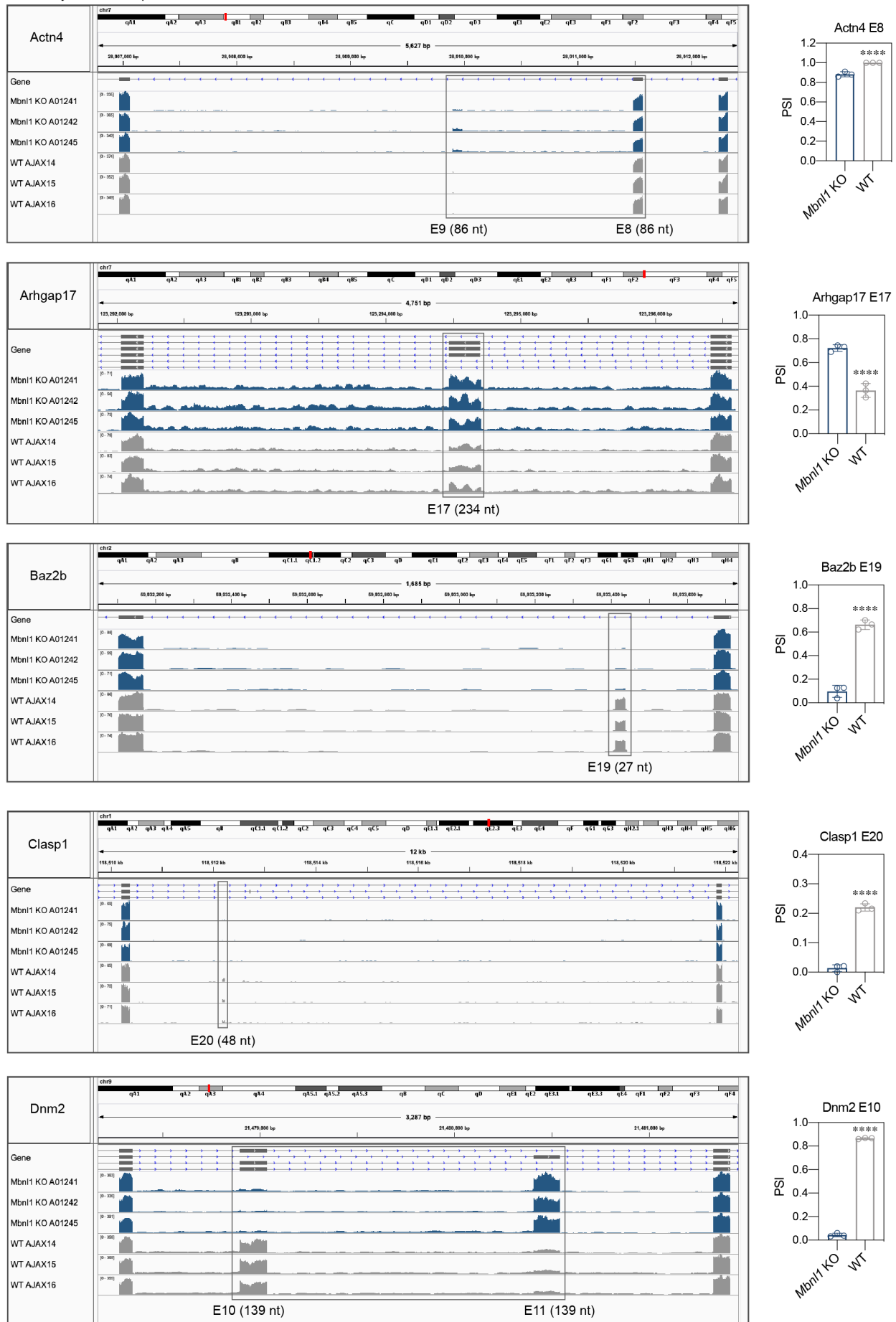
**h** Splenocyte composition at 4 (WT = 3; KO = 3), 8 (WT = 3; KO = 3) and ~22 (WT = 2; KO = 4) wks. CD4<sup>+</sup>, CD8<sup>+</sup>, CD4<sup>+</sup>CD8<sup>+</sup> double positive (DP) and CD4<sup>-</sup>CD8<sup>-</sup> double negative (DN) thymocytes were analyzed by flow cytometry. Graph represents mean KO - WT subpopulations  $\pm$  SD. Significant difference was determined by the two-tailed t-test: #  $P = 0.065$  (CD4<sup>+</sup>) and 0.079 (CD8<sup>+</sup>), \*\*  $P = 0.005$ .

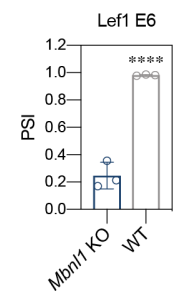
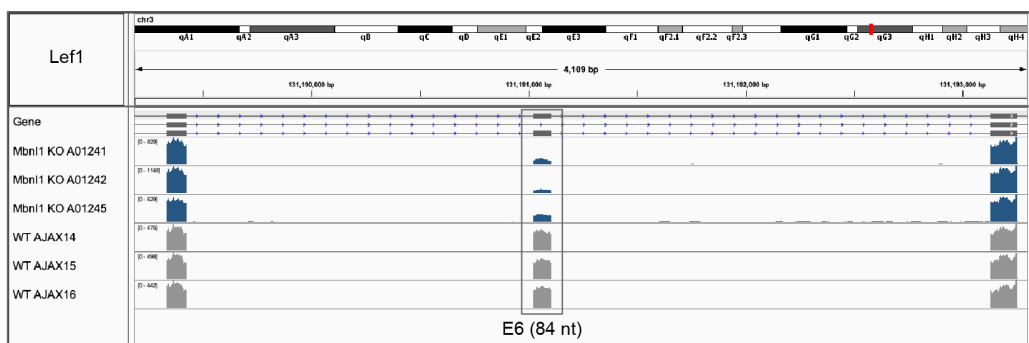
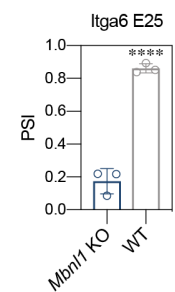
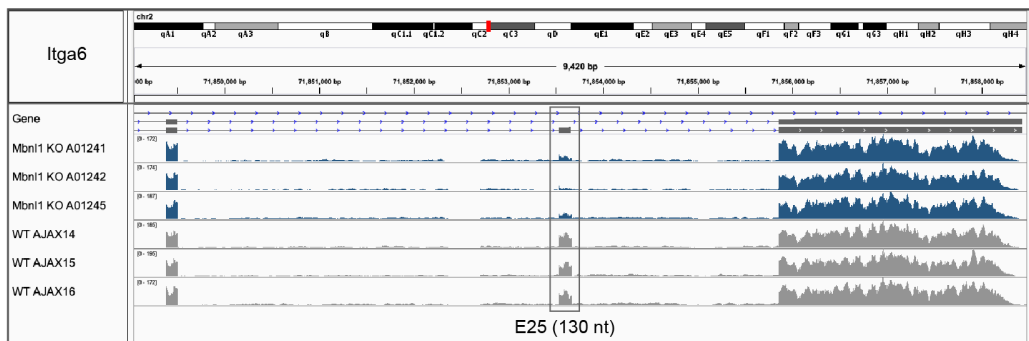
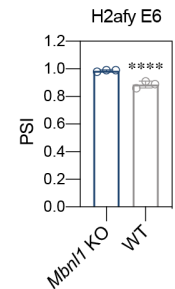
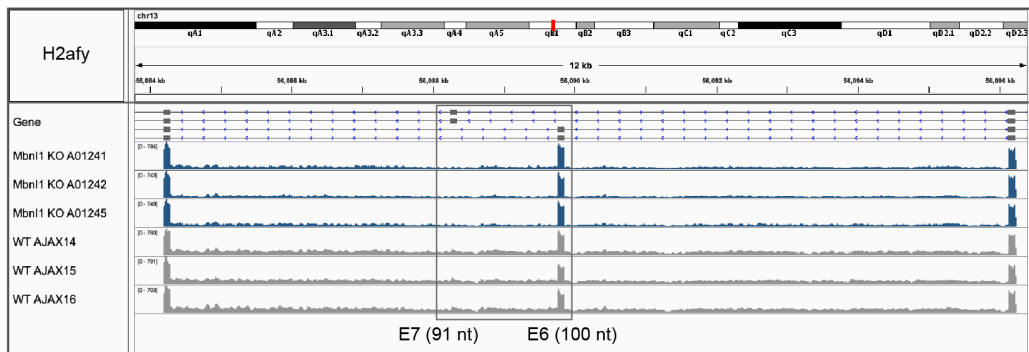
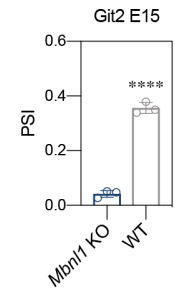
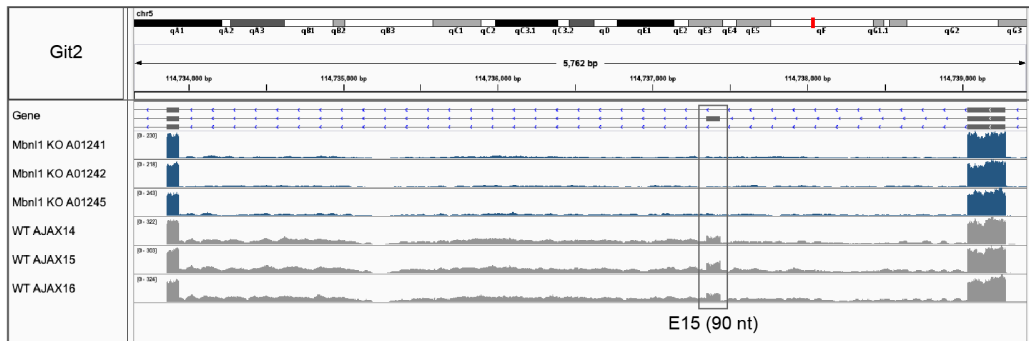
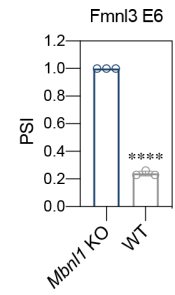
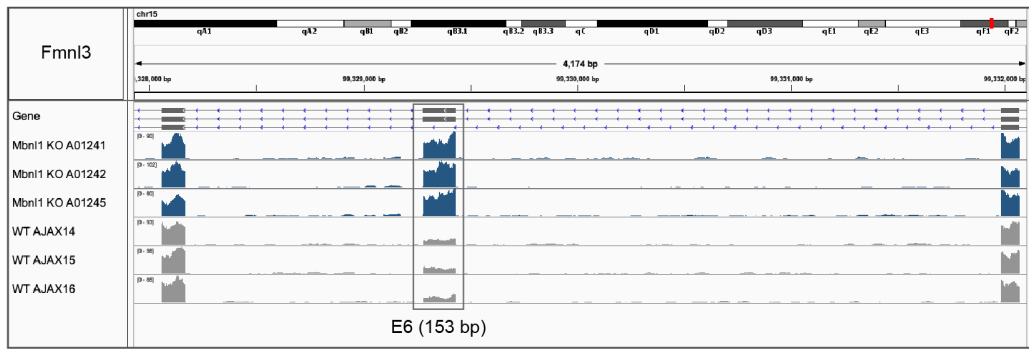
**i** Schematic of gating strategy for the flow cytometry analysis of dexamethasone-induced apoptosis.

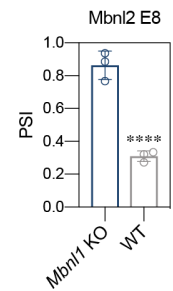
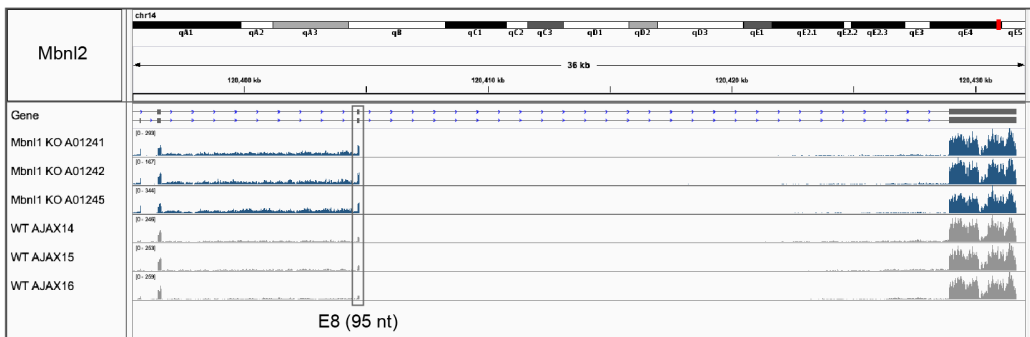
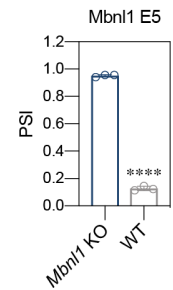
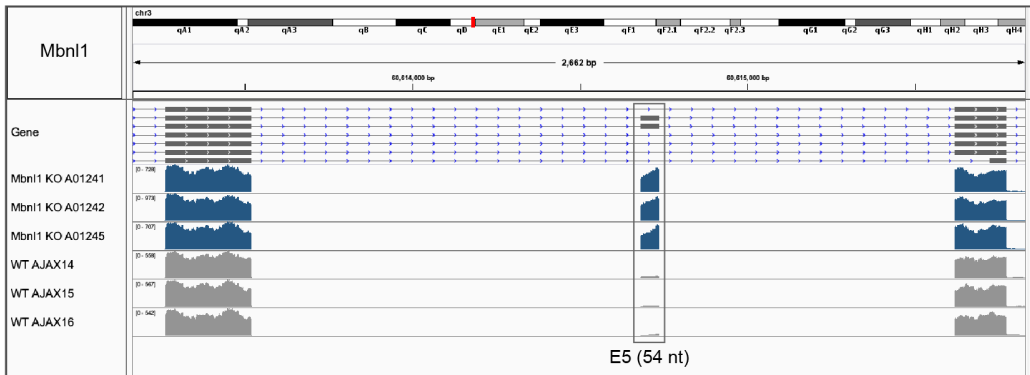
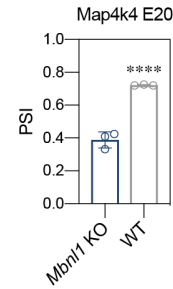
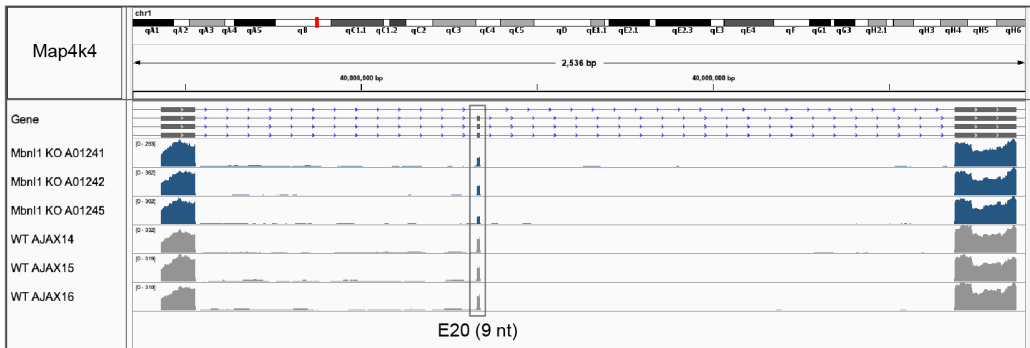
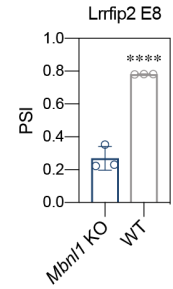
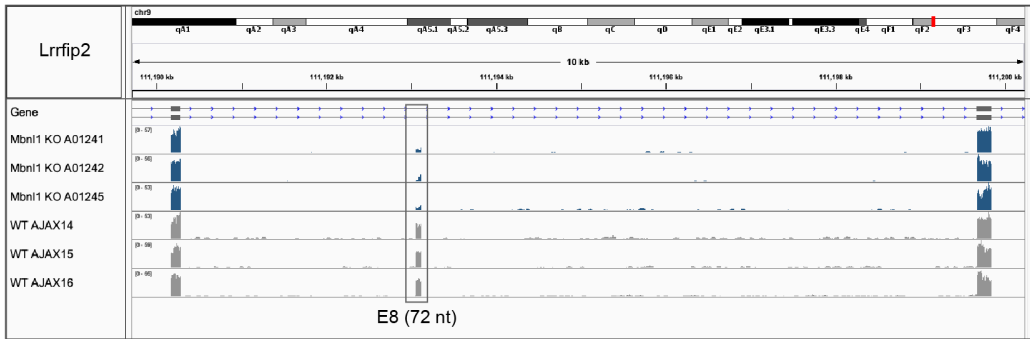
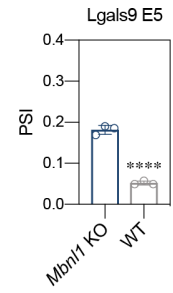
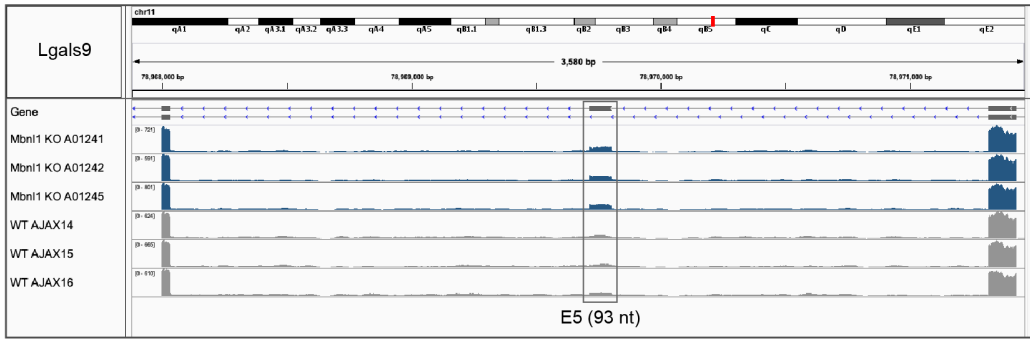
**j** Thymocytes derived from 4, 12 and ~22 wks 129-*Mbn1* KO mice (n = 3 for KO and WT at each time point) are resistant to 10<sup>-7</sup> M dexamethasone-induced apoptosis. Propidium iodide (PI) and Annexin V markers were used for early and late apoptosis, respectively. Results were normalized to untreated thymocytes derived from the same animal. Graph shows mean KO/WT fold change  $\pm$  SD. Significant difference was determined by two-tailed t-test test: \*  $P < 0.05$ , \*\*  $P < 0.01$ .

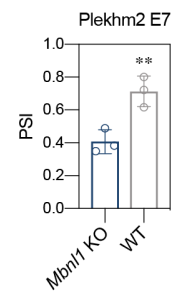
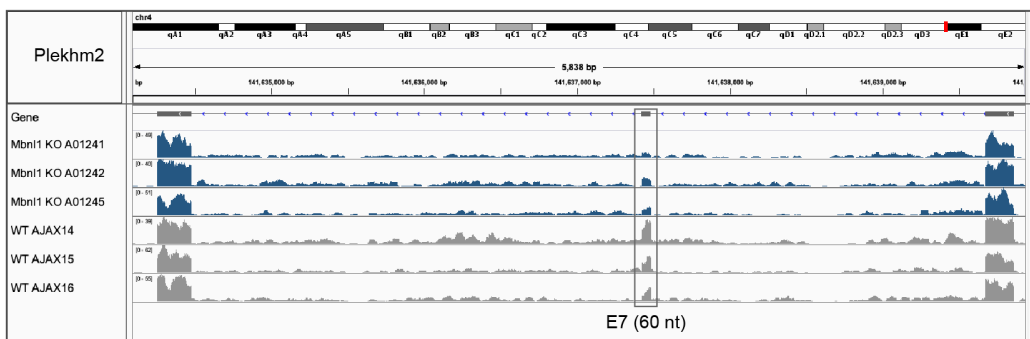
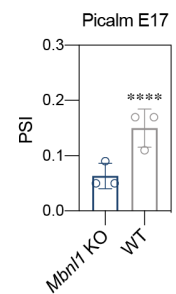
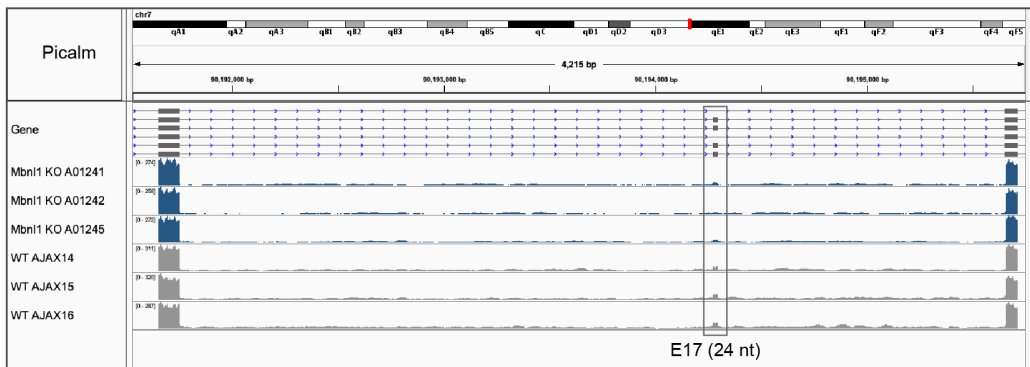
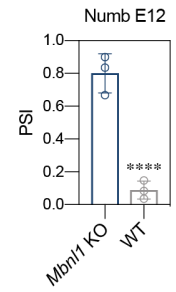
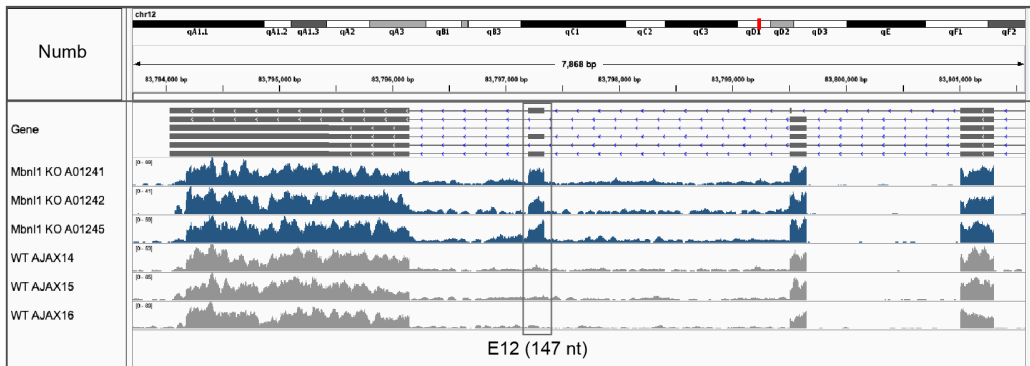
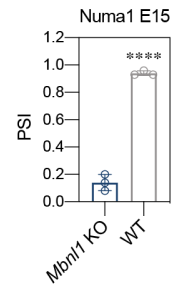
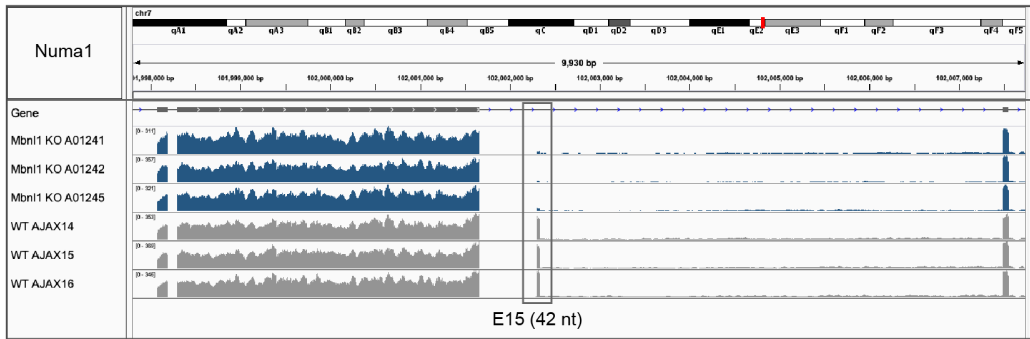
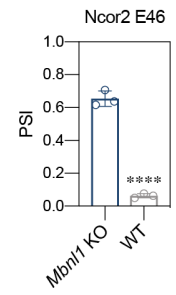
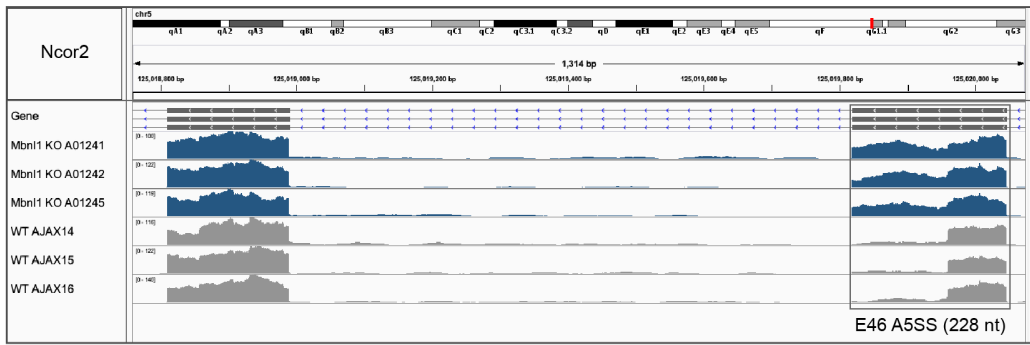
Source data are provided as a Supplementary Data 1 file.

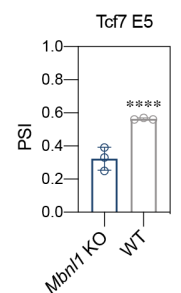
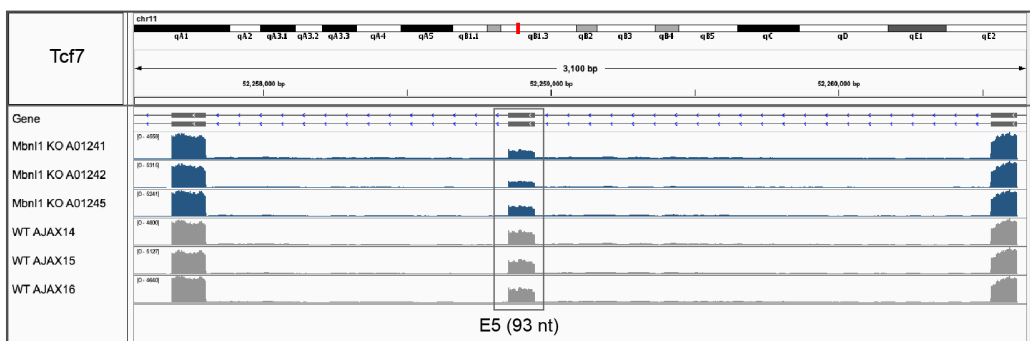
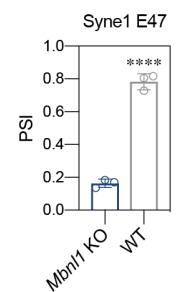
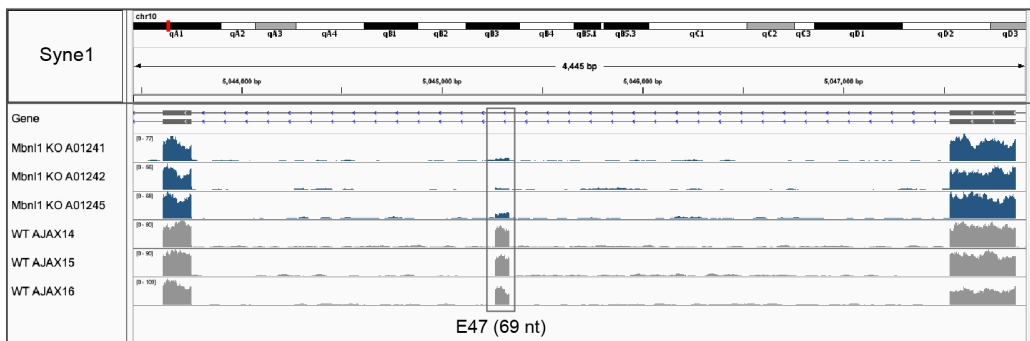
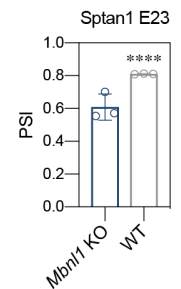
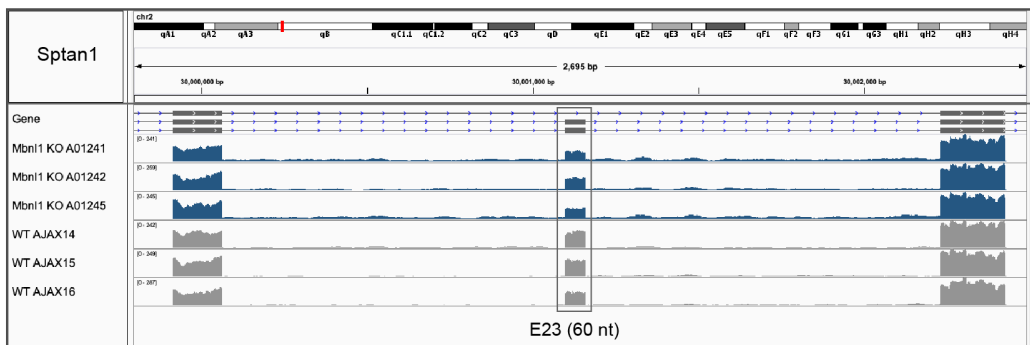
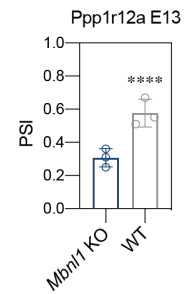
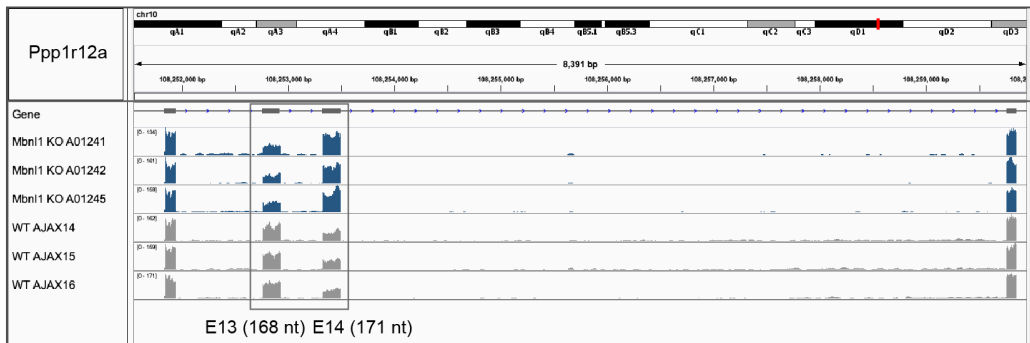
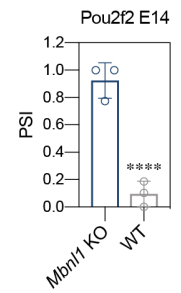
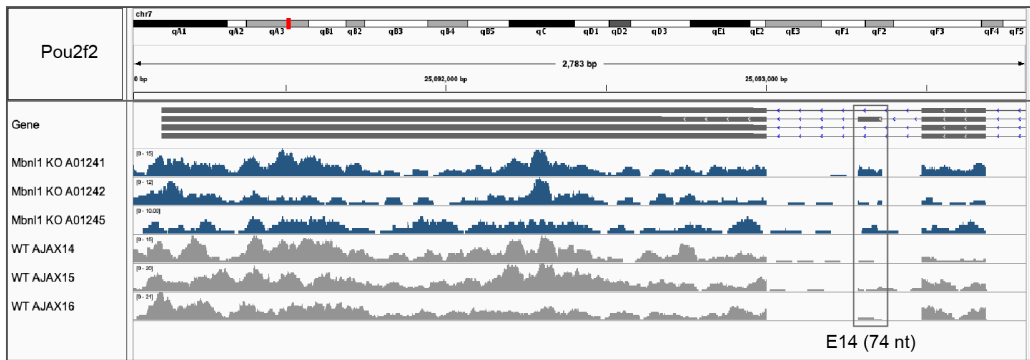
Mouse thymic RNA-seq

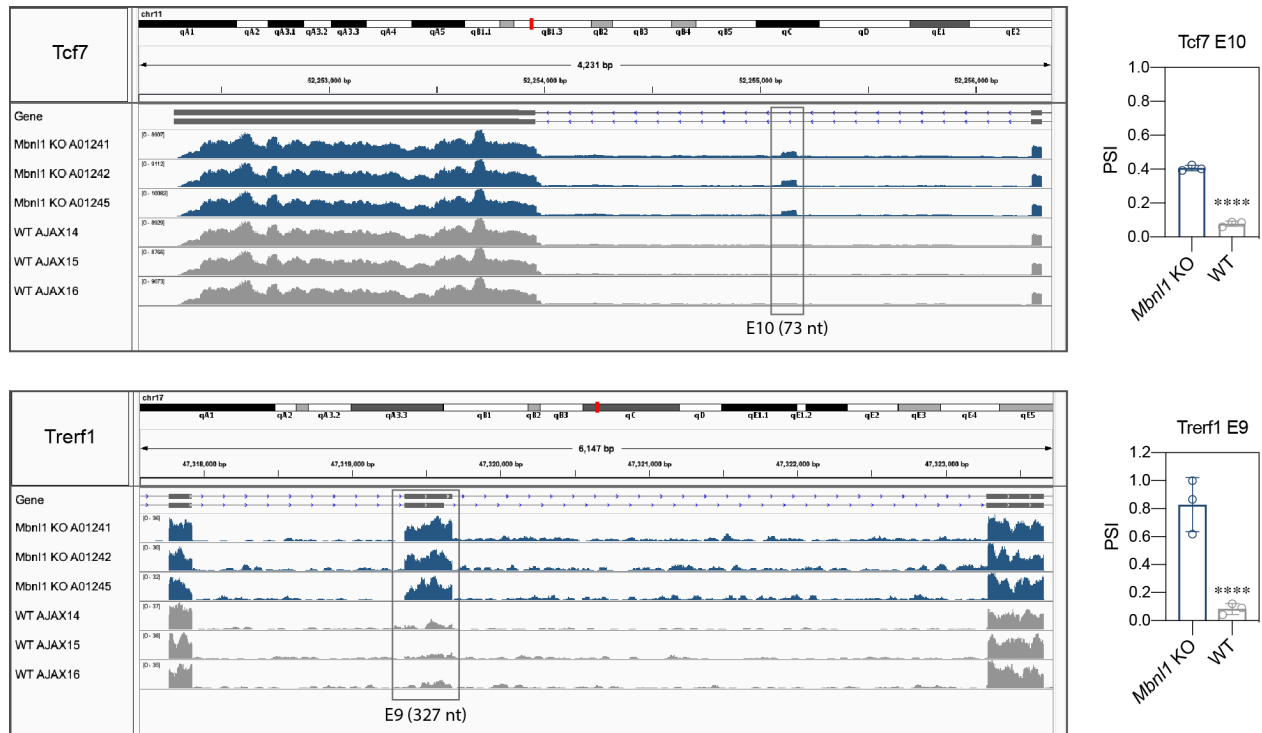










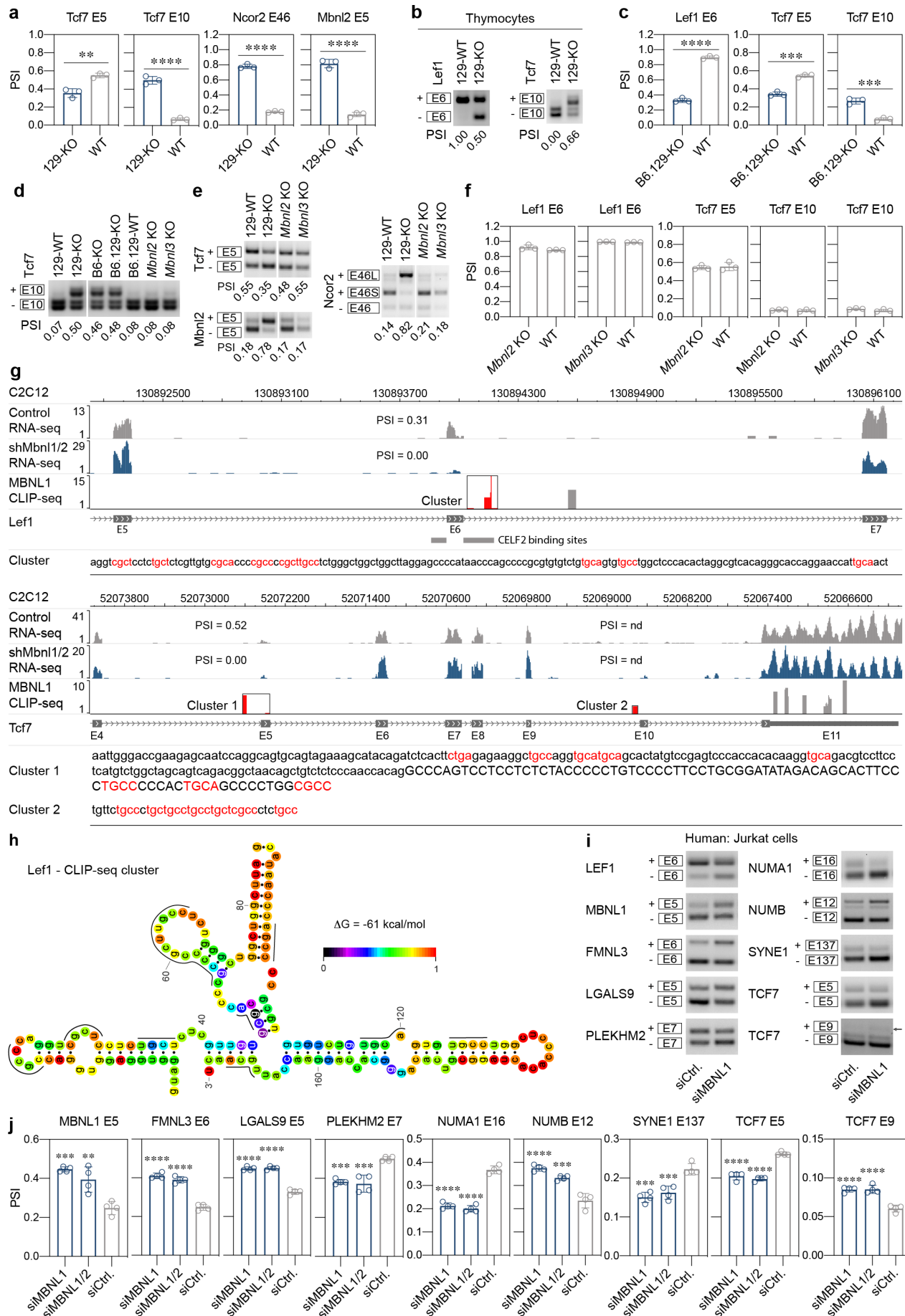


### Supplementary Fig. 3. Genome browser views of selected mouse alternative splicing events

Genome browser view of selected alternative splicing (AS) events from thymus *Mbn1* KO (n = 3) and WT (n = 3) RNA-seq data. *Mbn1* KO and WT are represented by blue and grey wiggle plots, respectively. Bar graphs show mean percent spliced in (PSI)  $\pm$  SD. rMATS; \*\* FDR < 0.01, \*\*\*\* FDR < 0.0001.

Source data are provided as a Supplementary Data 1 file.





#### Supplementary Fig. 4. MBNL1 directly regulates Lef1 E6

**a** Tcf7 E5, Tcf7 E10, Ncor2 E46 and Mbnl2 E5 splicing changes in 129-*Mbnl1* KO (n = 3) compared to WT (n = 3) thymi detected by RT-PCR. Bar graphs show mean PSI  $\pm$  SD. Significant differences were determined by the two-tailed t-test: \*\*  $P = 0.006$ , \*\*\*\*  $P < 0.0001$ .

**b** Representative gel of Lef1 E6 and Tcf7 E10 RT-PCR assays of thymocytes from 129-*Mbnl1* KO. Mean PSI values are indicated below the photo.

**c** Lef1 E6, Tcf7 E5 and Tcf7 E10 splicing changes in B6.129-*Mbnl1* KO (n = 3) compared to WT (n = 3) thymi detected by RT-PCR. Bar graphs show mean PSI  $\pm$  SD. Significant differences were determined by the two-tailed t-test: \*\*\*  $P = 0.0003$ , \*\*\*\*  $P < 0.0001$ .

**d** Representative gel of Tcf7 E10 RT-PCR assays of thymi from the different *Mbnl1* KO strains as well as *Mbnl2* and *Mbnl3* KOs. Mean PSI values are indicated below the photo.

**e** Representative gel of Tcf7 E5, Ncor2 E46 and Mbnl2 E5 RT-PCR assays of thymi from the *Mbnl1*, *Mbnl2* and *Mbnl3* KOs. Mean PSI values are indicated below the photo.

**f** Lef1 E6, Tcf7 E5 and Tcf7 E10 splicing changes in *Mbnl2* KO (n = 3), *Mbnl3* KO (n = 3) compared to WT (n = 3) thymi detected by RT-PCR. Bar graphs show mean PSI  $\pm$  SD. Significant difference were determined by the two-tailed t-test. There are no statistically significant differences.

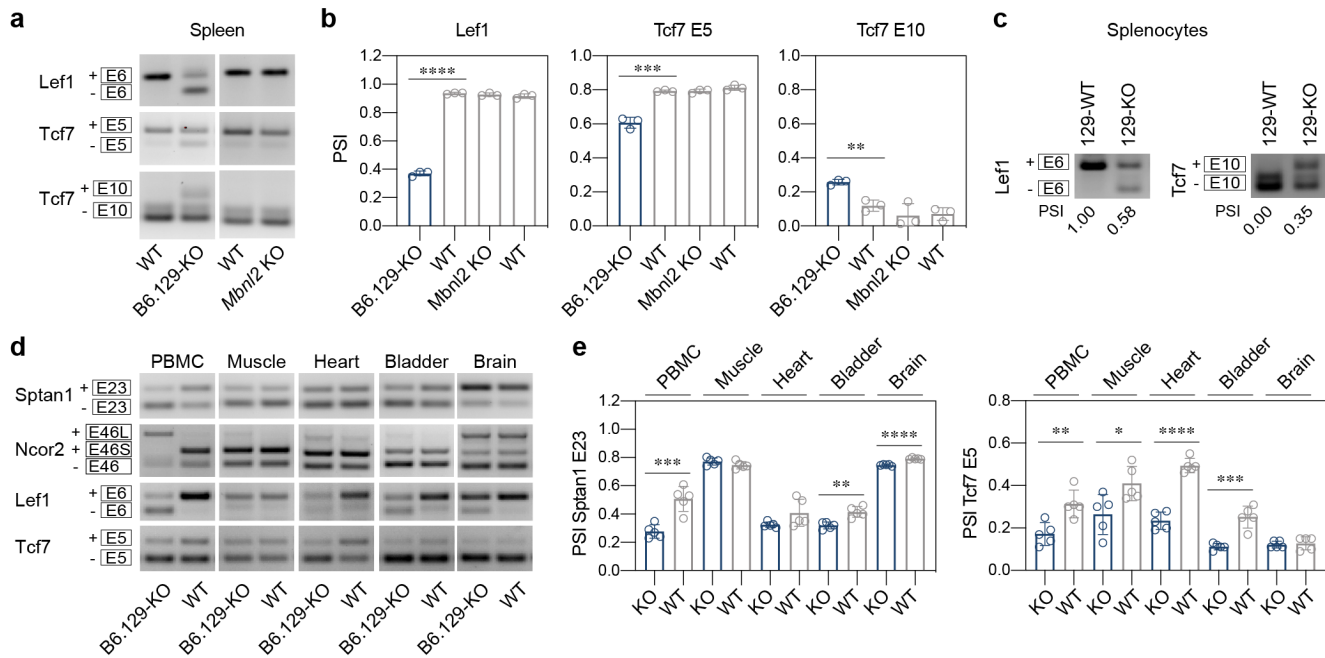
**g** Genome browser view of RNA-seq generated from C2C12 cells with compound Mbnl1 and Mbnl2 knock-down by shRNA. Cluster of MBNL1 CLIP-seq reads indicates MBNL1 binding sites in C2C12. YGCY/A motifs are marked (red). Predicted CELF2 binding sites are shown.

**h** Proposed secondary structure of the 5'-end of Lef1 intron 6 with potential MBNL1-binding motifs indicated (YGCY/A) (black line). The optimal thermodynamic stability of the structure is expressed in Gibbs free energy ( $\Delta G$ ) in kcal/mol for the reaction at 37°C using RNAfold software (<http://rna.tbi.univie.ac.at/>). The color annotation represents the pair probabilities of the nucleotides.

**i** Representative gel photos of AS events assessed by RT-PCR assays in human model of T cells (Jurkat) with MBNL1 knock-down by siRNA.

**j** MBNL1 (n = 4) and compound MBNL1 and MBNL2 (n = 4) knock-down causes AS changes in Jurkat cells. Bar graphs show mean PSI  $\pm$  SD. The significant differences were determined by Dunnett's multiple comparison test: \*\*  $P_{adj} < 0.01$ , \*\*\*  $P_{adj} < 0.001$ , \*\*\*\*  $P_{adj} < 0.0001$ . Note that LEF1 E6 graph is Fig. 3i.

Source data are provided as the Source Data and Supplementary Data 1 files.



### Supplementary Fig. 5. Alternative splicing changes in *Mbn1* KO splenocytes and PBMCs

**a** Representative gel of Lef1 E6 and Tcf7 E5 RT-PCR assays on spleen isolated from the 129-*Mbn1* KO and WT.

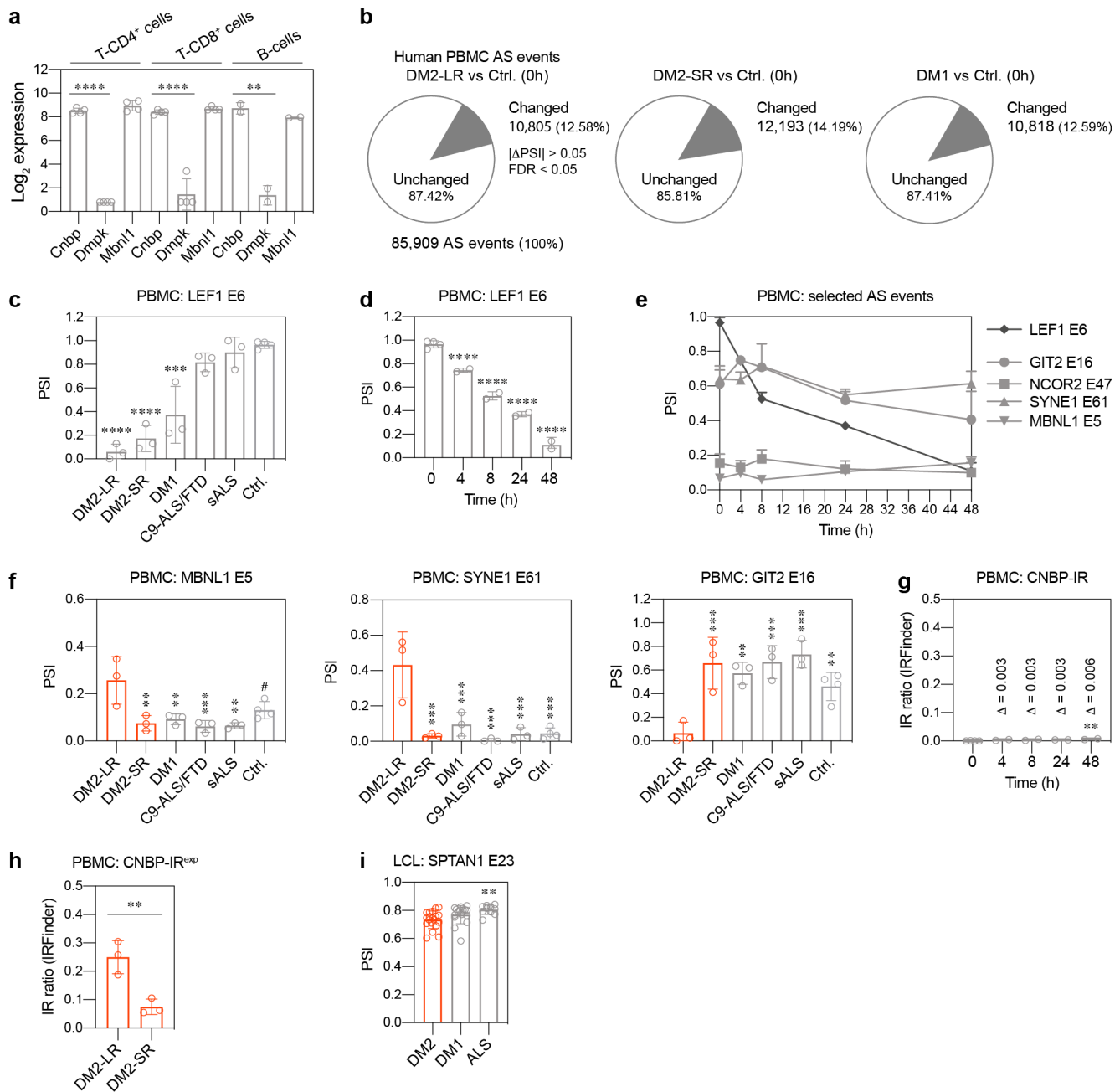
**b** Lef1 E6, Tcf7 E5 and Tcf7 E10 splicing changes in B6.129-*Mbn1* KO (n = 3) compared to WT (n = 3) spleens detected by RT-PCR. Bar graphs show mean PSI  $\pm$  SD. Significant differences were determined by the two-tailed t-test: \*\*\*  $P = 0.0006$ , \*\*\*\*  $P < 0.0001$ .

**c** Representative gels of Lef1 E6 and Tcf7 E10 RT-PCR assays on splenocytes isolated from the 129-*Mbn1* KO (n = 2) and WT. Mean PSI values are provided below the photo.

**d** Representative gels of AS events assessed by RT-PCR assays on B6.129-*Mbn1* KO and WT PBMCs, muscle (tibialis anterior), heart, bladder and brain.

**e** B6.129-*Mbn1* KO (n = 5) causes the same AS changes in PBMCs, muscle, heart, bladder and brain. Bar graphs show mean PSI  $\pm$  SD. Significant differences were determined by the two-tailed t-test test: \*  $P < 0.05$ , \*\*  $P < 0.01$ , \*\*\*  $P < 0.001$ , \*\*\*\*  $P < 0.0001$ .

Source data are provided as the Source Data and Supplementary Data 1 files.



## Supplementary Fig. 6. Alternative splicing changes in DM2 PBMCs

**a** *Cnbp*, *Dmpk* and *Mbnl1* expression in mouse T-CD4<sup>+</sup> cells (B220<sup>-</sup>, CD3<sup>+</sup>, CD19<sup>-</sup>, CD4<sup>+</sup>, CD8<sup>-</sup>), T-CD8<sup>+</sup> cells (B220<sup>-</sup>, CD3<sup>+</sup>, CD19<sup>-</sup>, CD4<sup>-</sup>, CD8<sup>+</sup>) and B-cells (B220<sup>+</sup>, CD3<sup>-</sup>, CD19<sup>+</sup>). Gene expression obtained from the BloodSpot database (servers.binf.ku.dk/bloodspot)<sup>2</sup>; Dataset: Mouse Normal (RNA-seq) - GSE60101. Bar graph shows mean expression  $\pm$  SD. Significant differences were determined by the two-tailed t-test: \*\*  $P < 0.008$ , \*\*\*\*  $P < 0.0001$ .

**b** Delayed PBMC isolation results in transcriptomic changes. Pie charts represent the proportion of significantly changed AS events (gray triangle) to all detected AS events in DM2-LR ( $n = 3$ ), DM2-SR ( $n = 3$ ) and DM1 ( $n = 3$ ) PBMC RNA-seq samples. RNA-seq from freshly isolated (0h) PBMCs was used as a control - GSE58335<sup>3</sup>.

**c** LEF1 E6 is significantly excluded in DM2-LR, DM2-SR and DM1 RNA-seq data. Bar graph shows mean PSI  $\pm$  SD. Significant difference was determined by Dunnett's multiple comparison test: \*\*\*  $P_{adj} = 0.0001$ , \*\*\*\*  $P_{adj} < 0.0001$ .

**d** Delayed PBMC isolation leads to significant exclusion of LEF1 E6 in unaffected PBMCs. Bar graph shows mean PSI  $\pm$  SD. rMATS; \*\*\*\* FDR < 0.0001.

**e** Four AS events resistant to change caused by delayed PBMC isolation. Selected AS events were analyzed in this study and there were no significant changes between 0h and 4/8/24/48 hrs. Points connected by lines show mean PSI  $\pm$  SD.

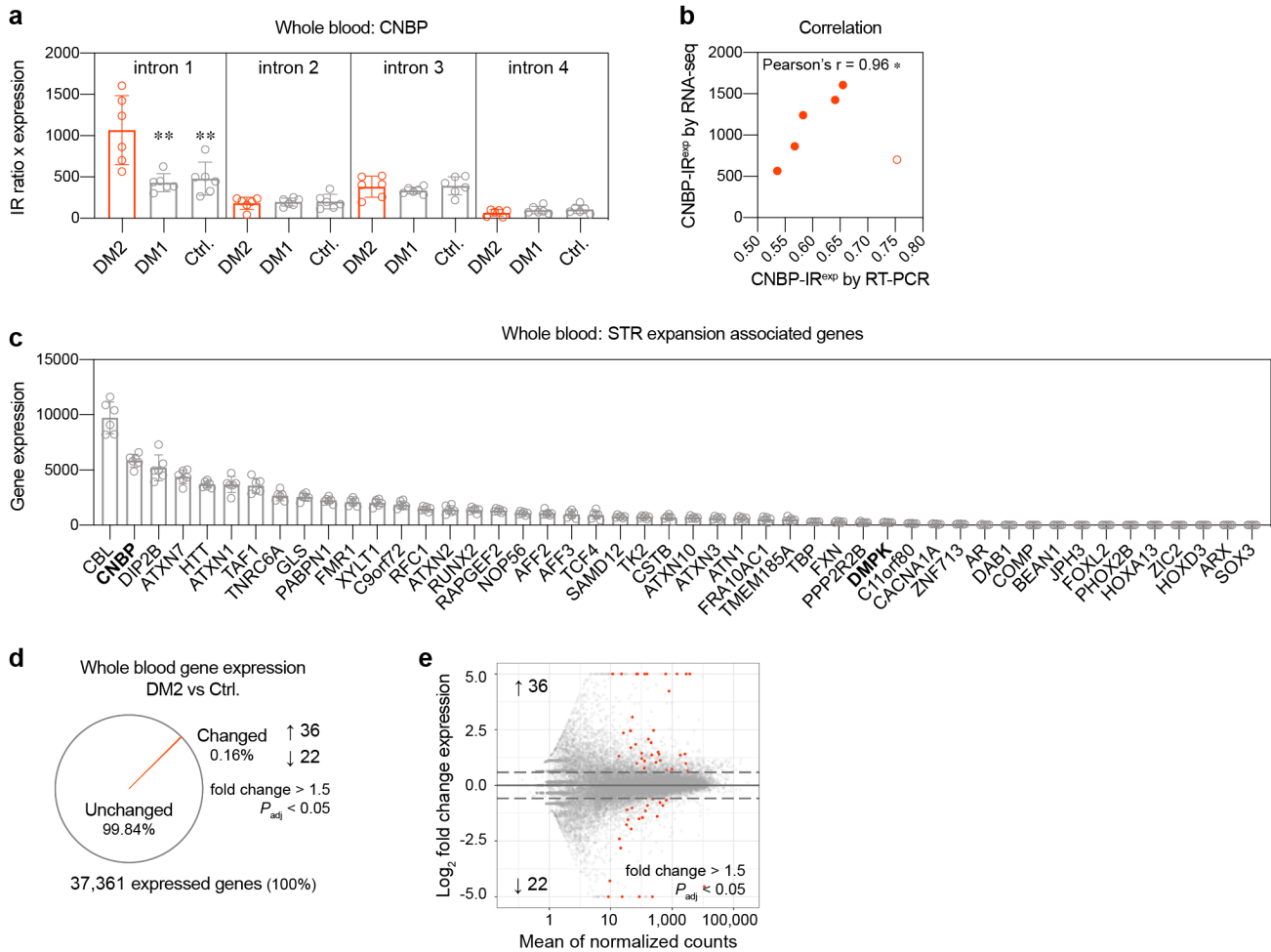
**f** Aberrant MBNL1 E5, SYNE1 E61 and GIT2 E16 splicing in DM2-LR but not in DM2-SR, DM1, C9-ALS/FTD nor sALS RNA-seq PBMC samples. Bar graphs show mean PSI  $\pm$  SD. Significant difference were determined by Dunnett's multiple comparisons test: #  $P_{adj} = 0.157$ , \*\*  $P_{adj} < 0.01$ , \*\*\*  $P_{adj} < 0.001$ .

**g** Delayed PBMC isolation does not affect CNBP intron 1 retention (CNBP-IR) in unaffected samples. Bar graph shows mean IR ratio  $\pm$  SD. Significant difference was determined by Dunnett's multiple comparison test: \*\*  $P_{adj} = 0.009$ .

**h** Significant differences in CNBP-IR<sup>exp</sup> between DM2-LR and DM2-SR. Bar graph shows mean IR ratio  $\pm$  SD. Significant difference was determined by the two-tailed t-test test: \*\*  $P = 0.009$ .

**i** Aberrant SPTAN1 E23 exclusion in a large cohort of DM2-derived LCLs (n = 19); DM1 (n = 16); ALS (n = 10). Bar graph shows mean PSI  $\pm$  SD. Significant difference was determined by Dunn's multiple comparison test: \*\*  $P_{adj} = 0.003$ .

Source data are provided as a Supplementary Data 1 file.



## Supplementary Fig. 7. Gene expression changes in DM2 whole blood

**a** *CNBP* intron 1, 2, 3 and 4 retention analysis in DM2 ( $n = 6$ ), DM1 ( $n = 6$ ) and unaffected control ( $n = 6$ ) samples. Bar graph shows mean IR ratio x *CNBP* expression  $\pm$  SD. Significant difference was determined by Dunnett's multiple comparisons test:  $** P_{adj} < 0.004$ .

**b** Correlation between *CNBP*-IR<sup>exp</sup> measured by RT-PCR (Fig. 4a) and RNA-seq (Supplementary Fig. 7a). One sample (circle) was excluded from the analysis because 5-times less total RNA (200 ng) was used for library preparation and the sequencing depth was relatively low (29 million uniquely mapped reads).  $* P = 0.01$ .

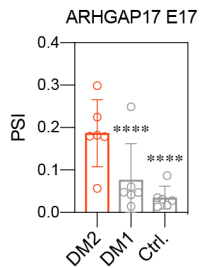
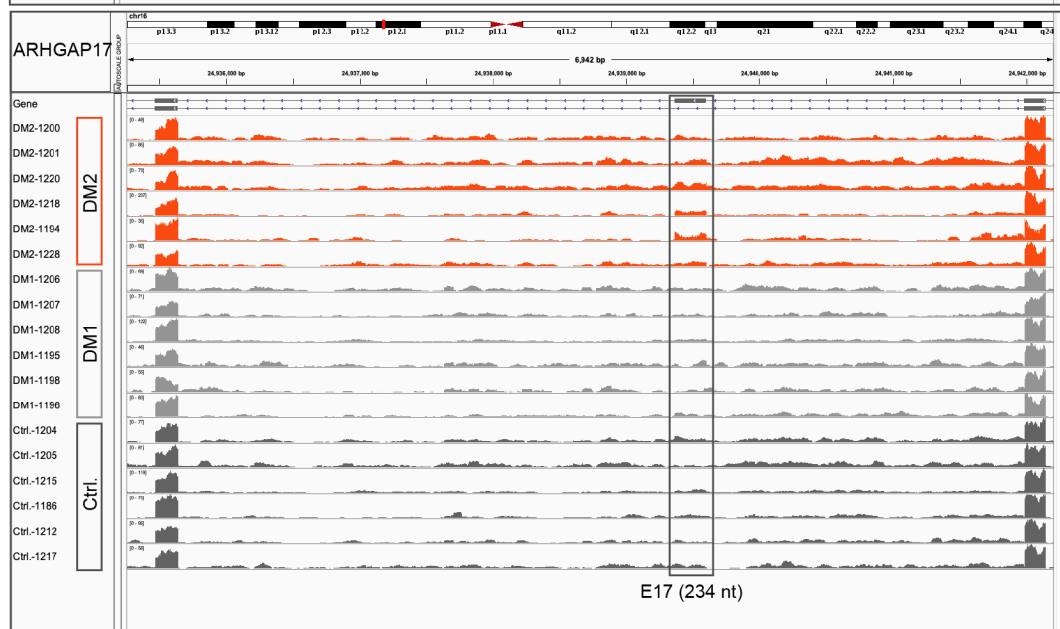
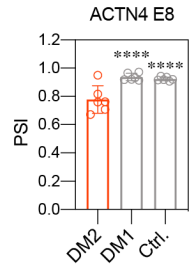
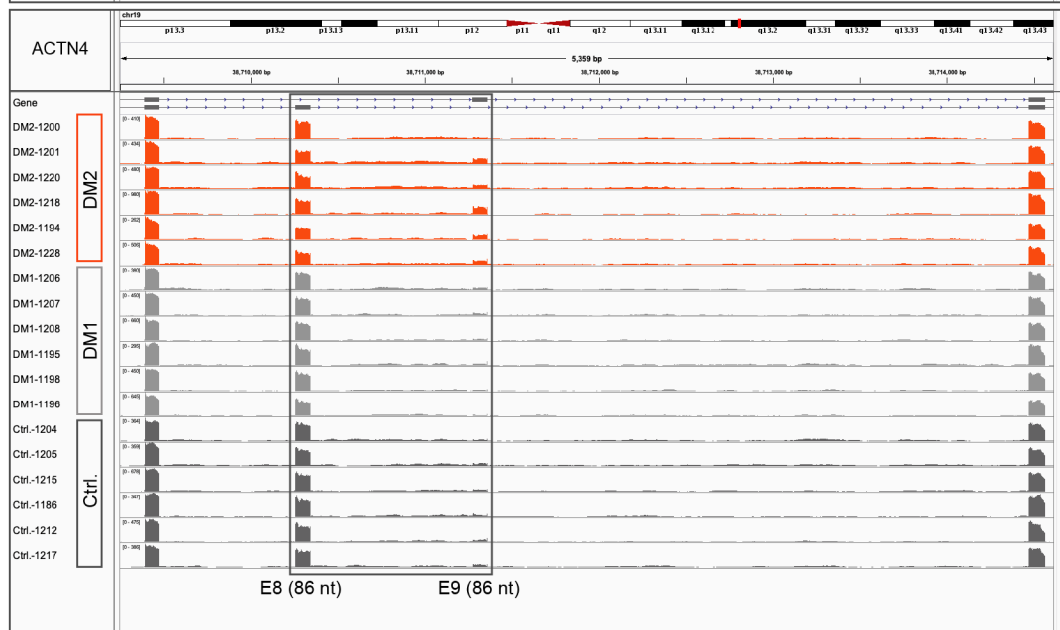
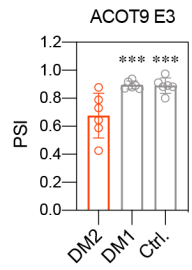
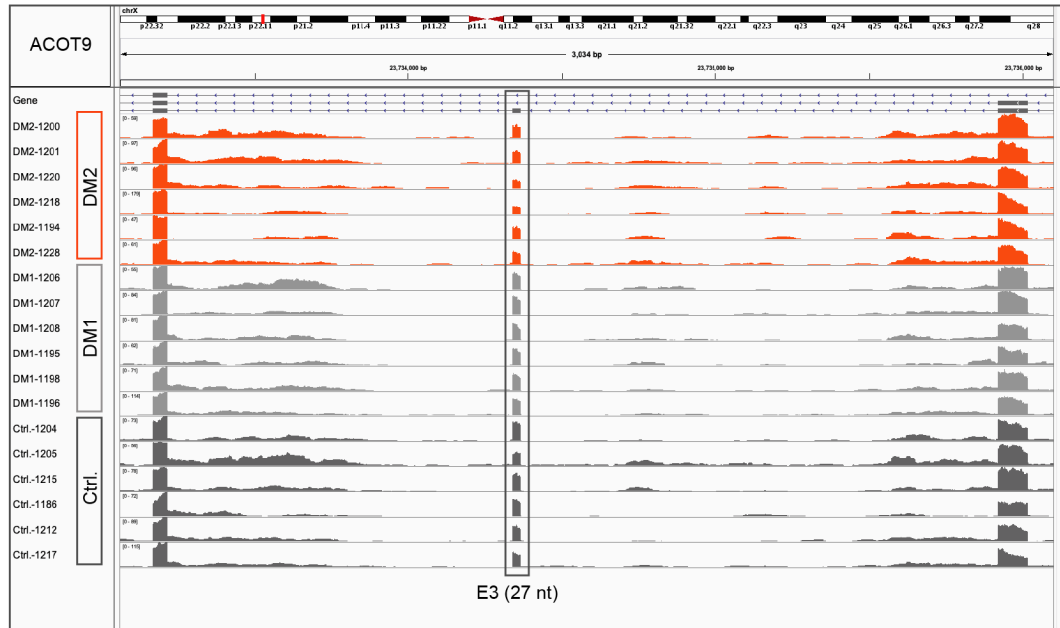
**c** Expression of microsatellite expansion associated genes in unaffected whole blood RNA-seq samples. Bar graph shows mean expression  $\pm$  SD.

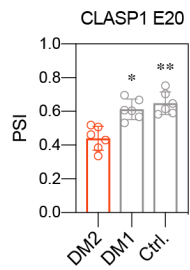
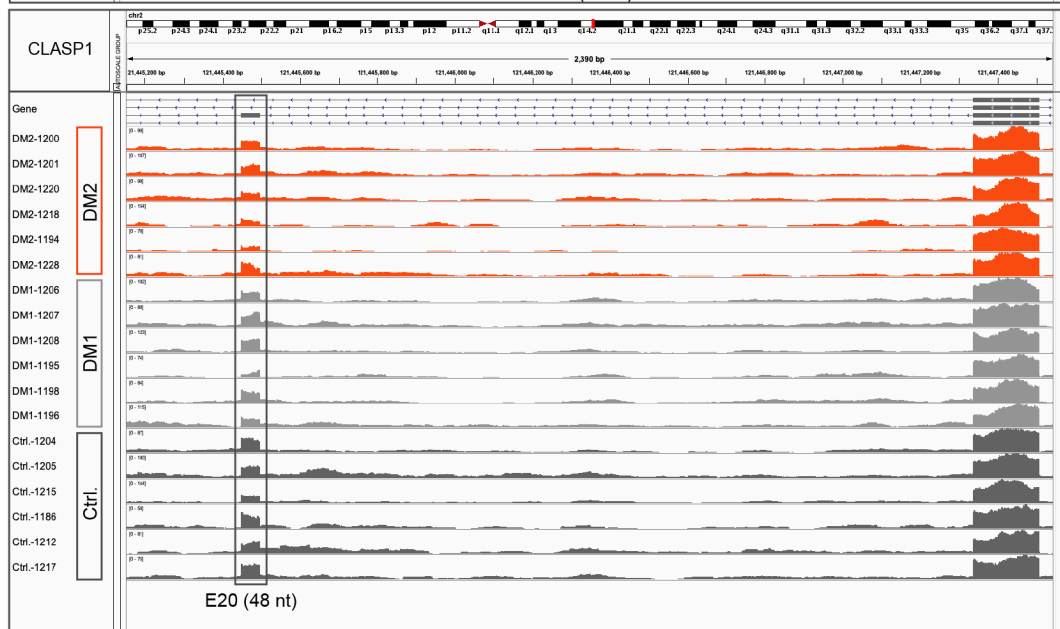
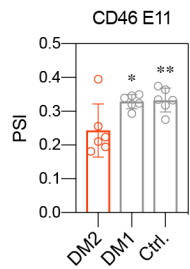
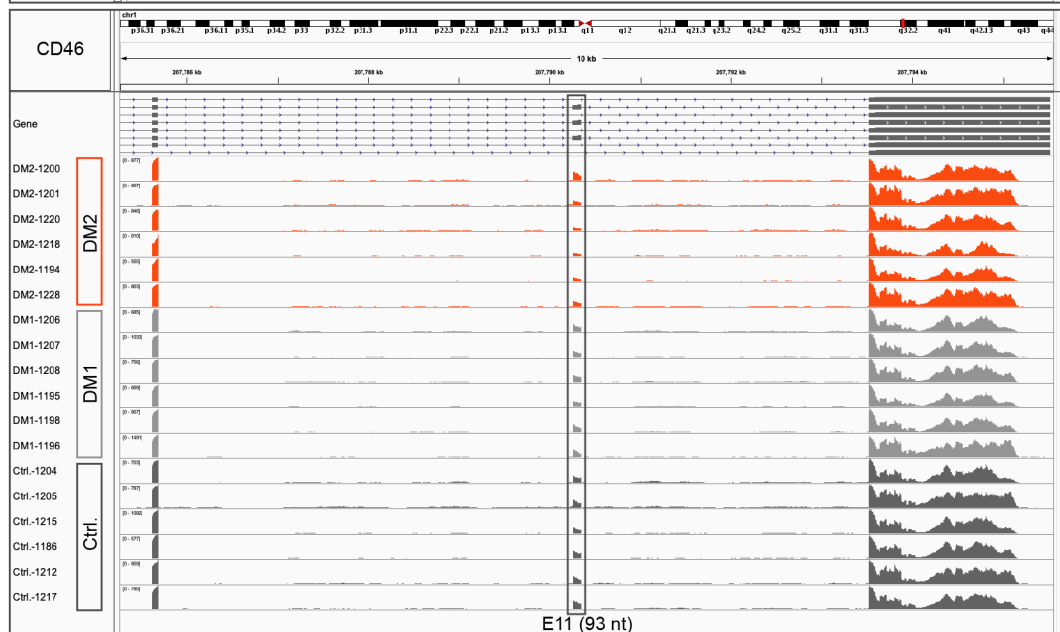
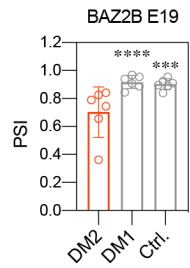
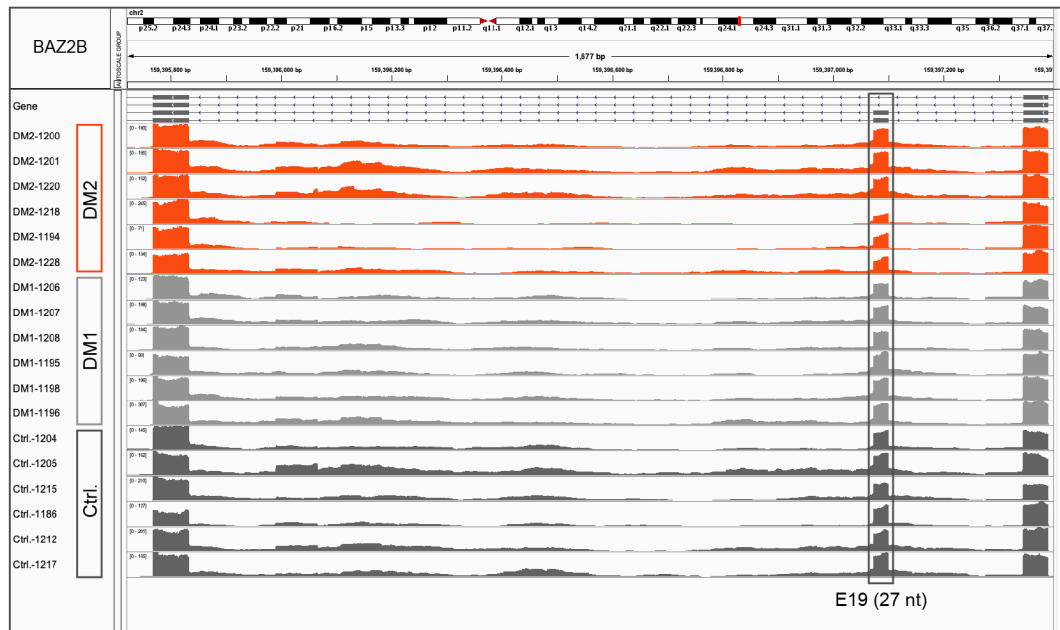
**d** Gene expression changes in DM2 whole blood. Pie chart represents the proportion of significantly altered genes (orange) to all detected genes (gray) in DM2 ( $n = 6$ ) compared to unaffected control ( $n = 6$ ) RNA-seq samples.

**e** Differential gene expression analysis for DM2 whole blood ( $n = 6$ ). Orange dots on the volcano plot represent significantly different expressed genes in DM2 compared to unaffected control whole blood samples.

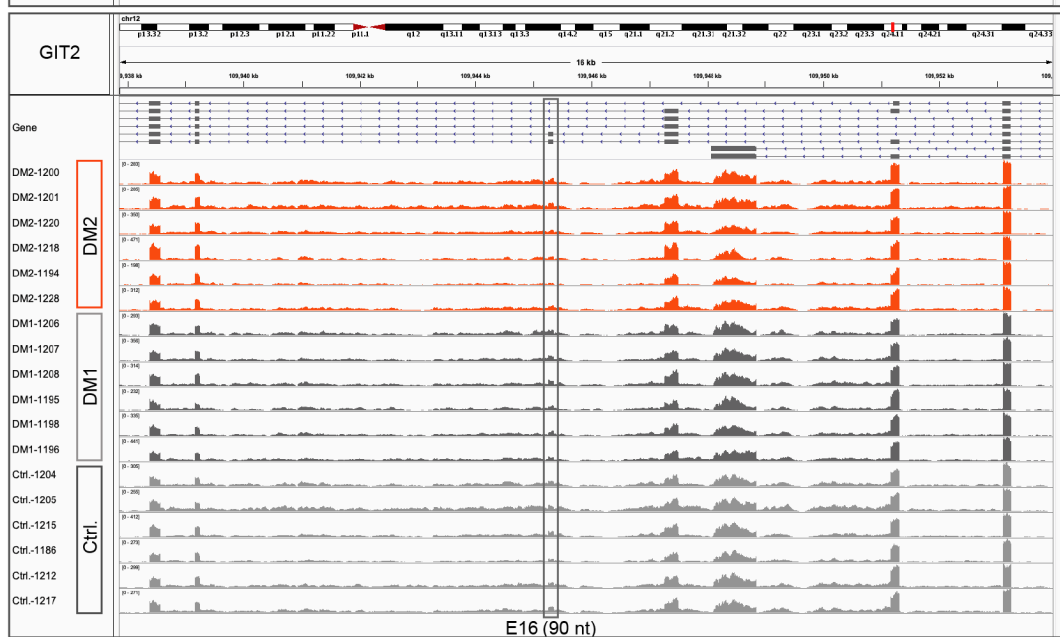
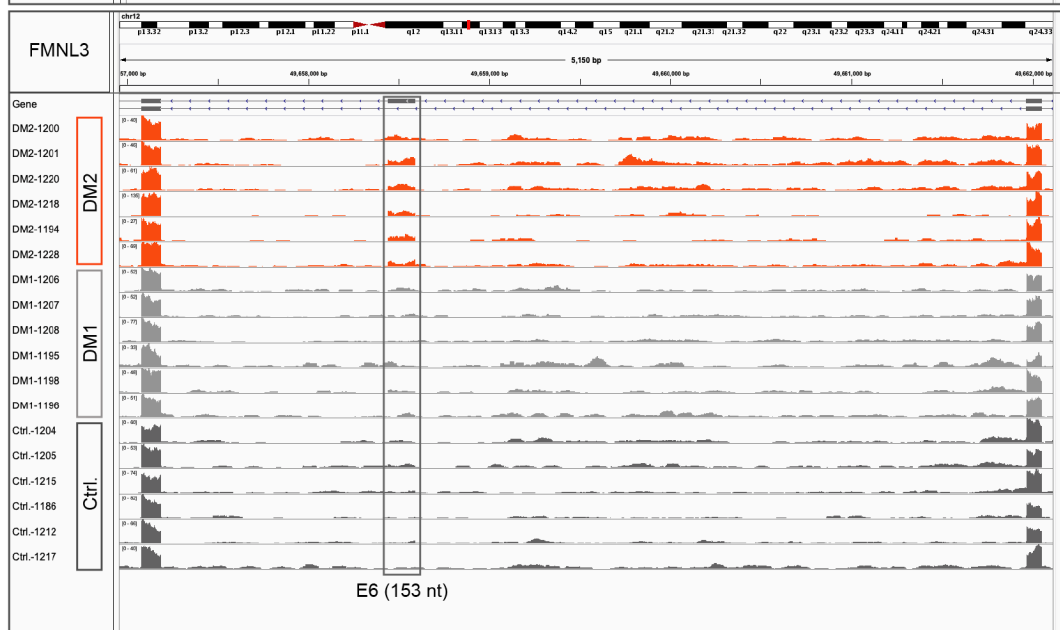
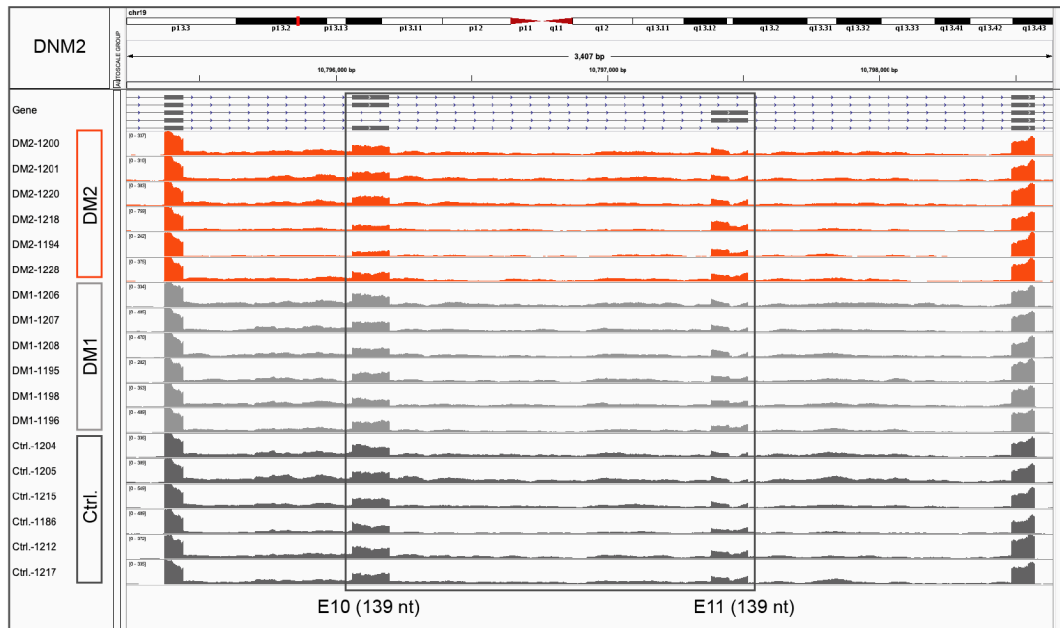
Source data are provided as a Supplementary Data 1 file.

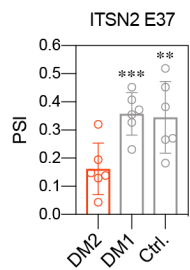
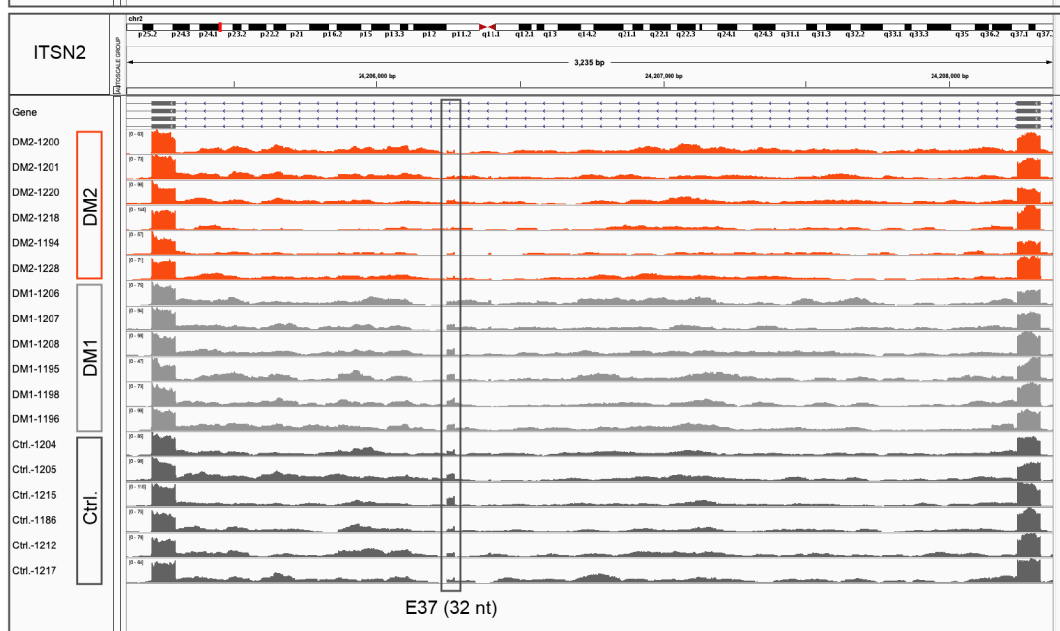
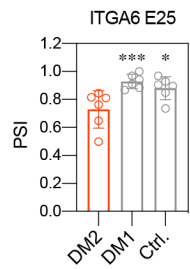
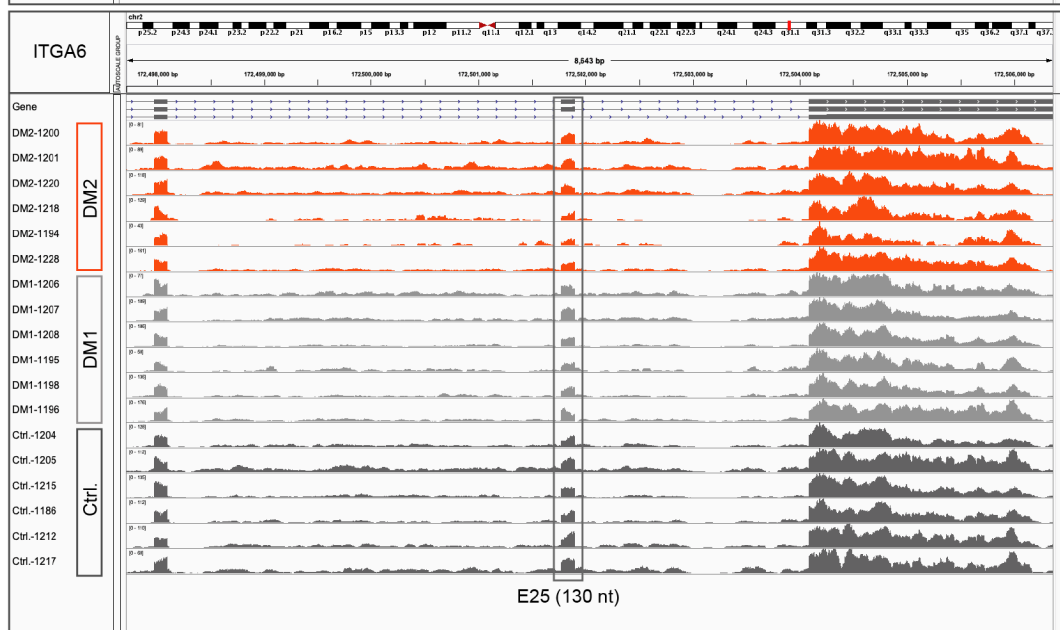
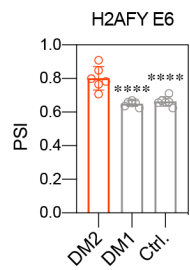
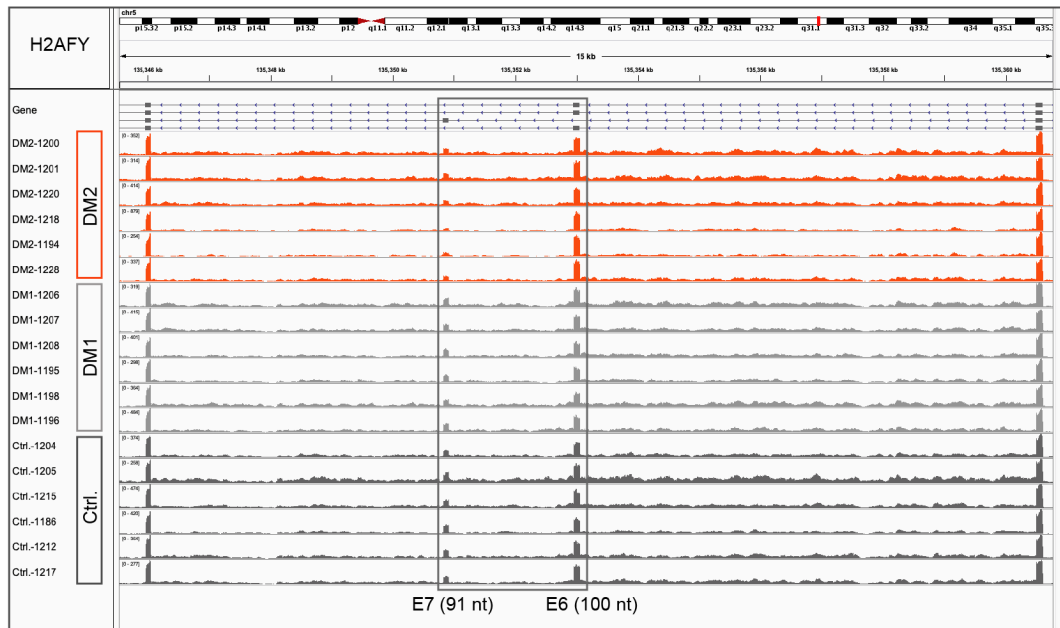
Human whole blood RNA-seq

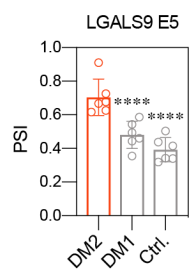
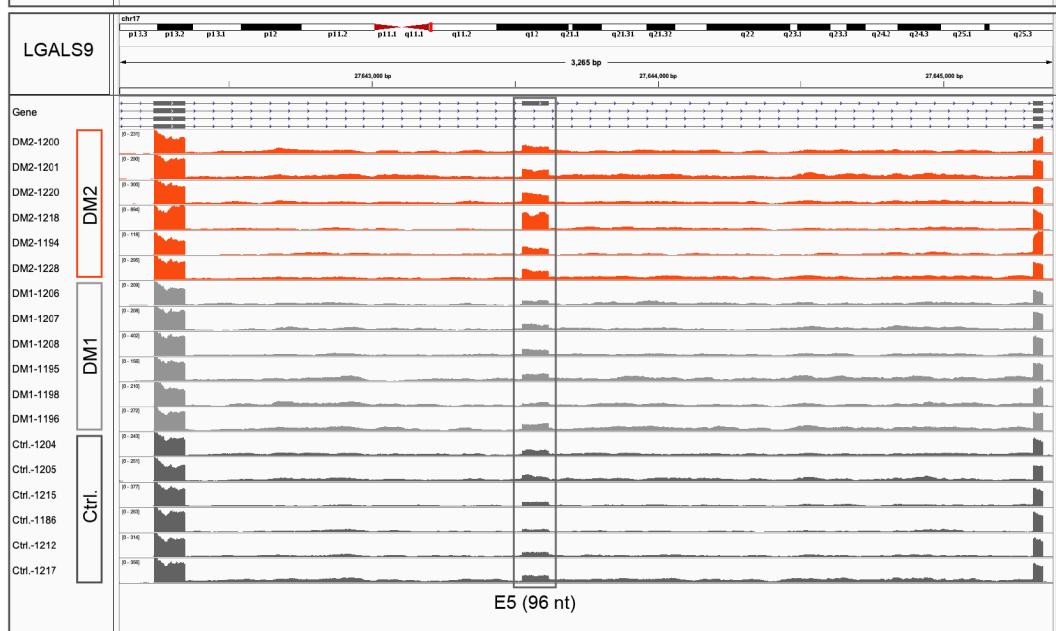
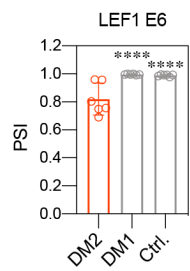
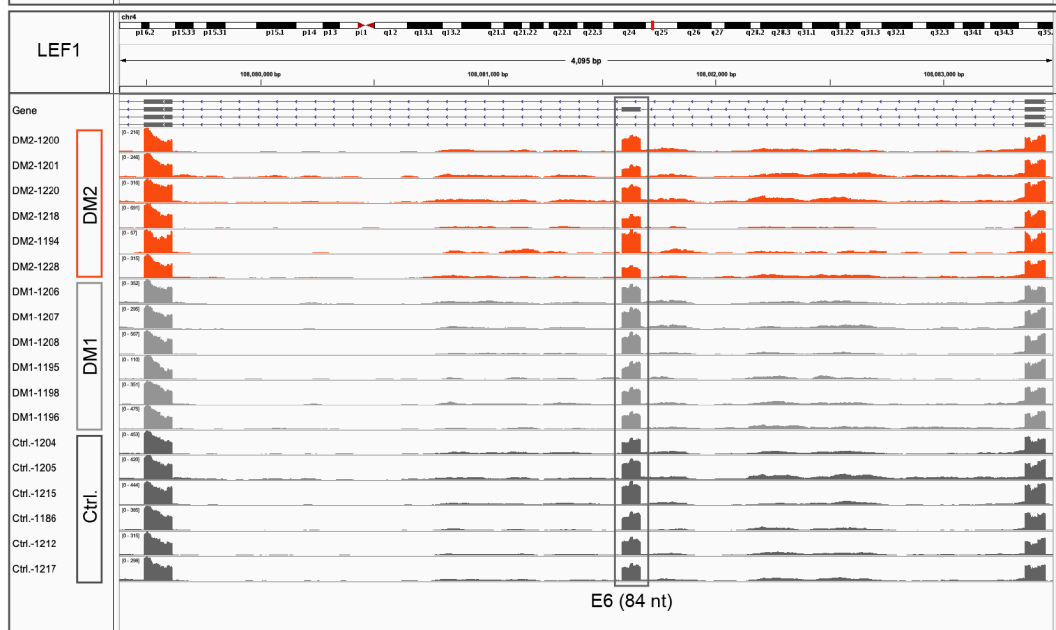
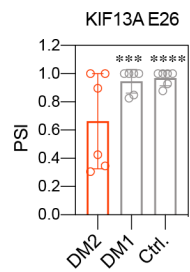
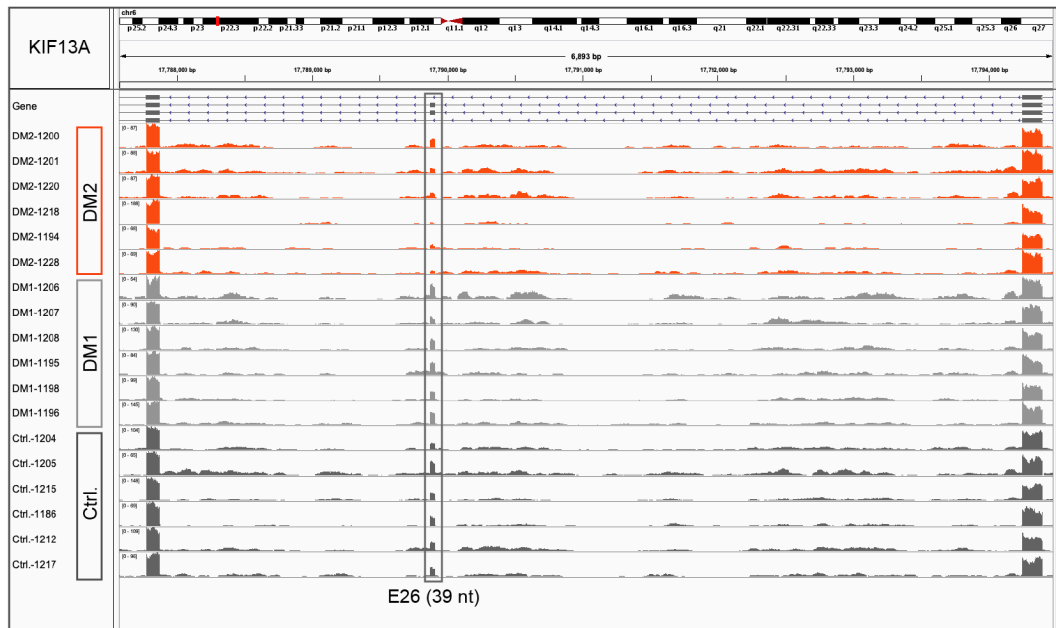




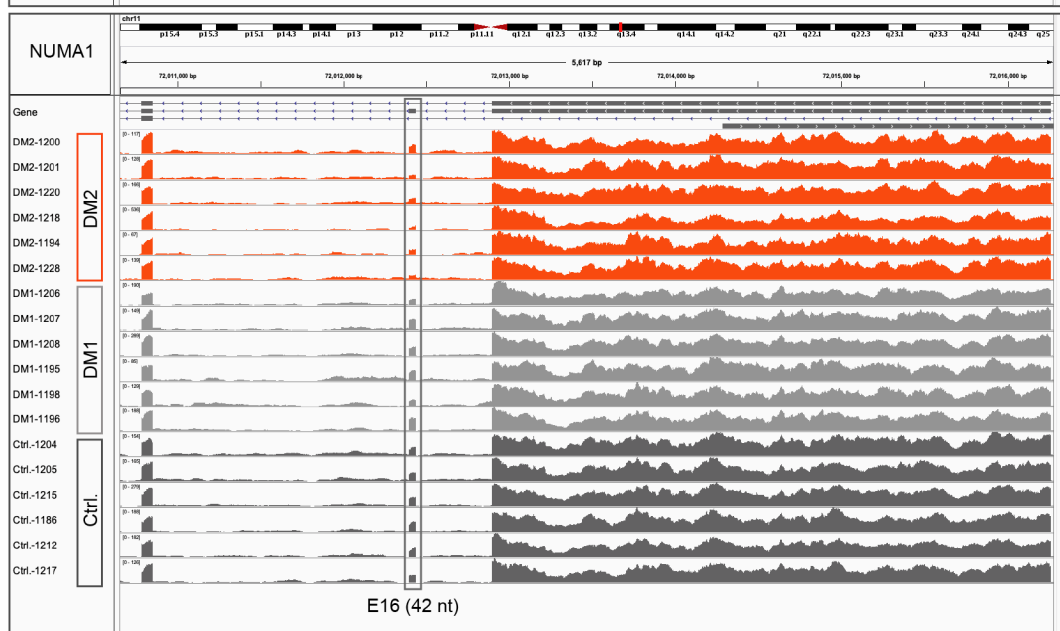
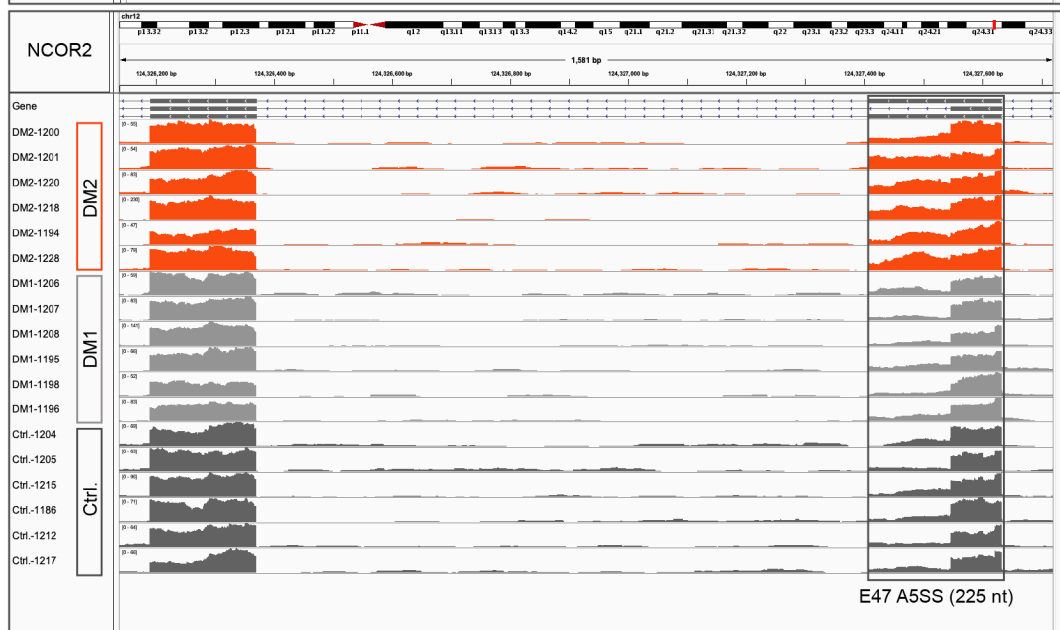
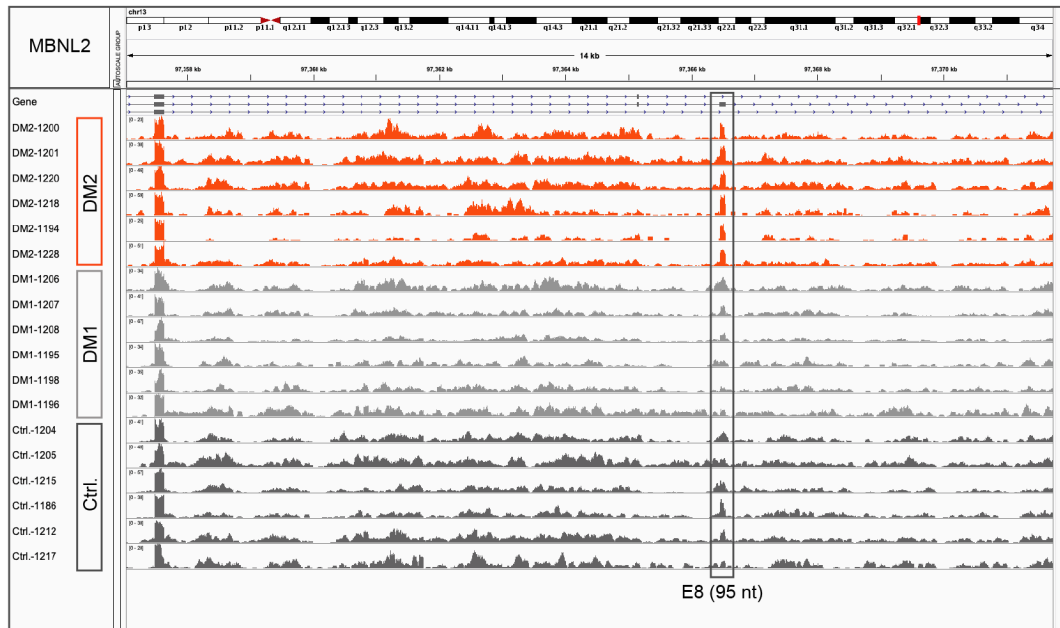


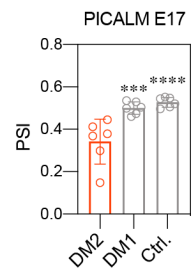
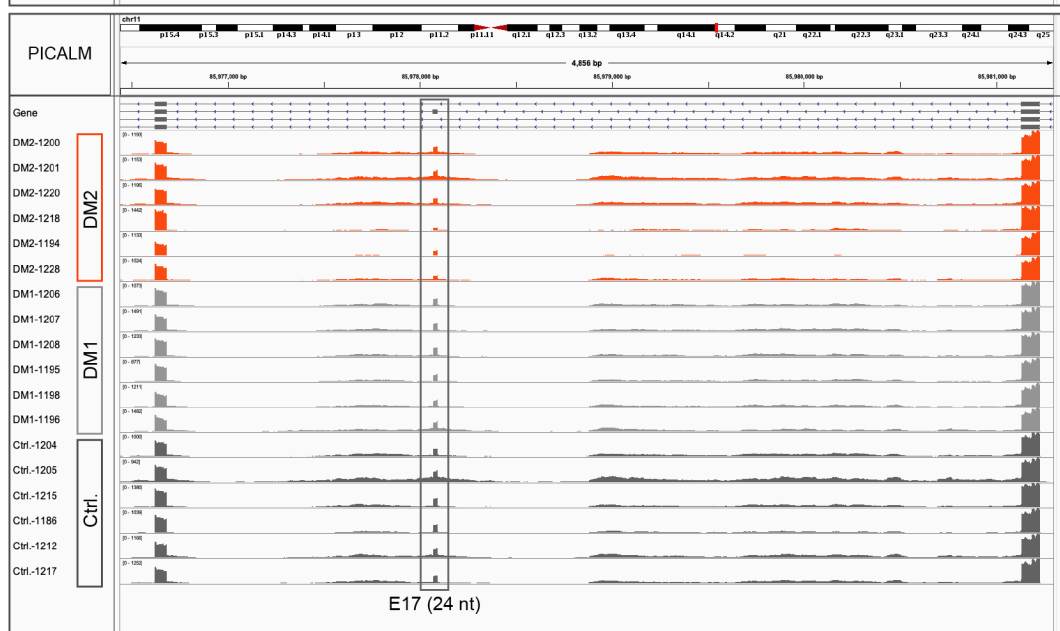
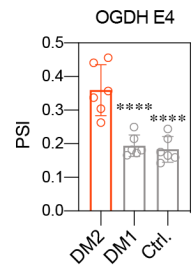
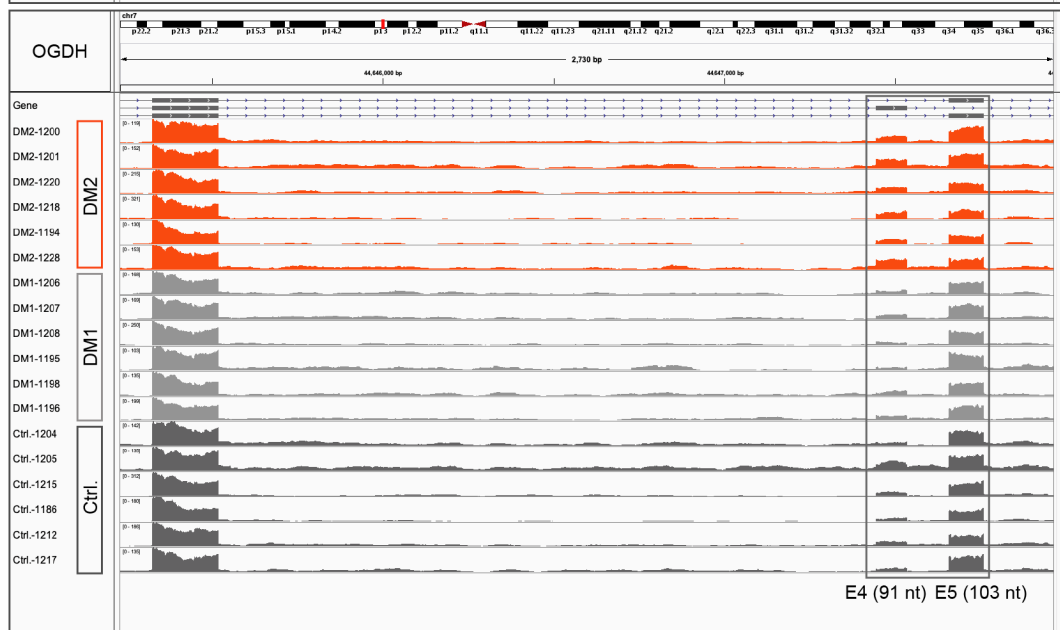
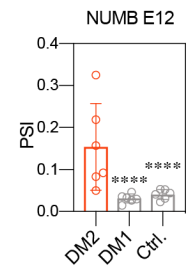
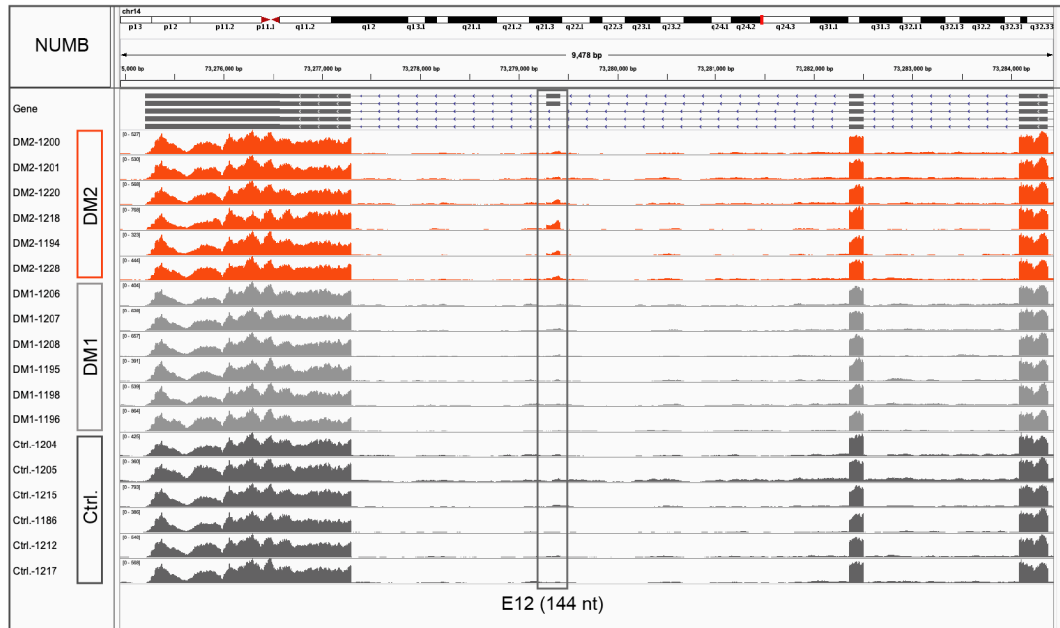


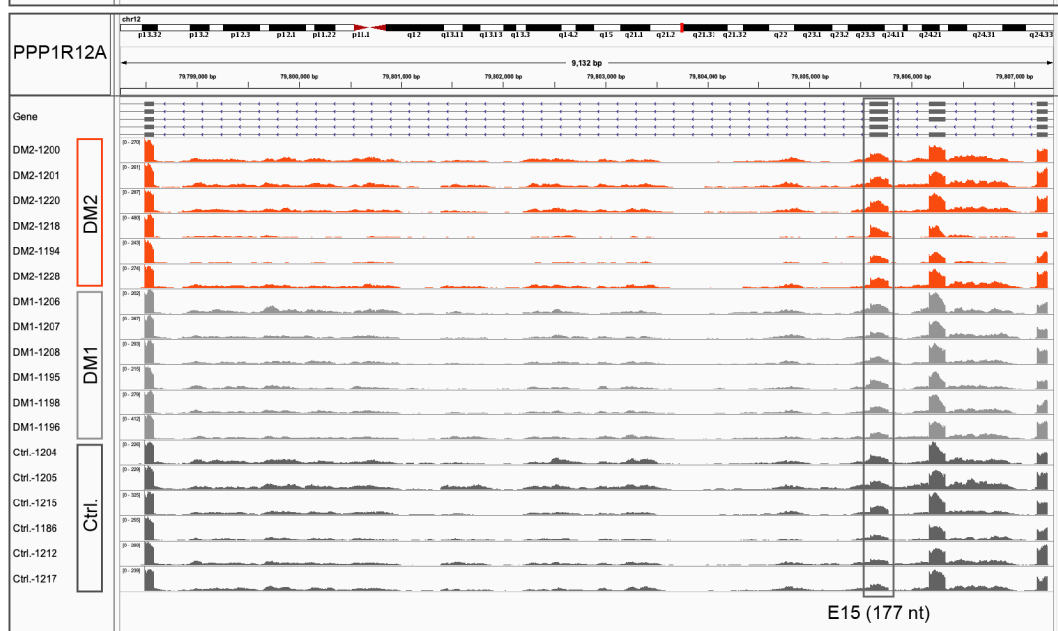
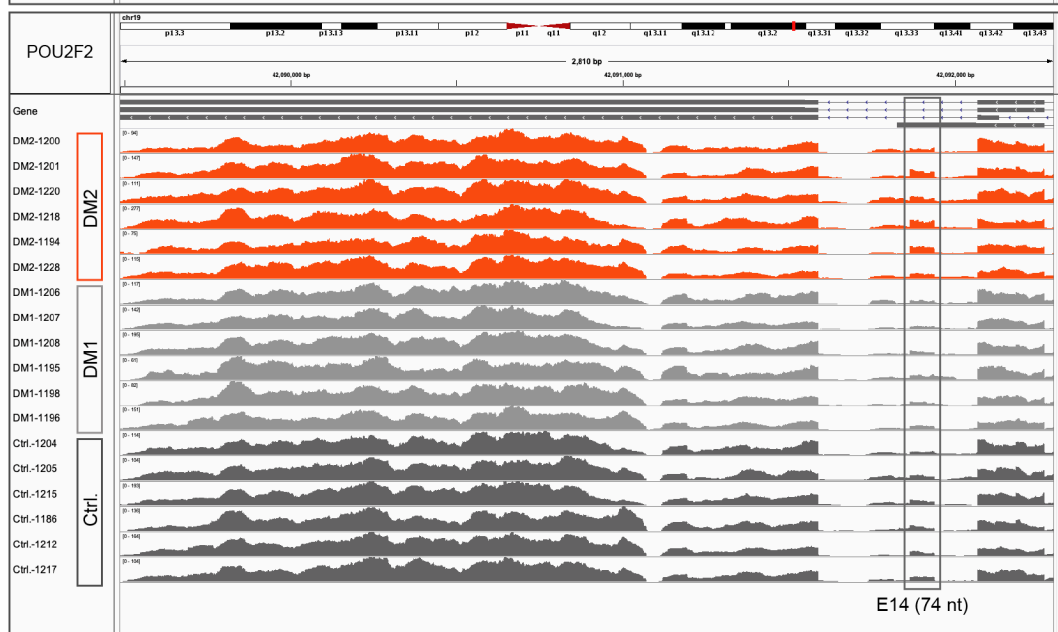
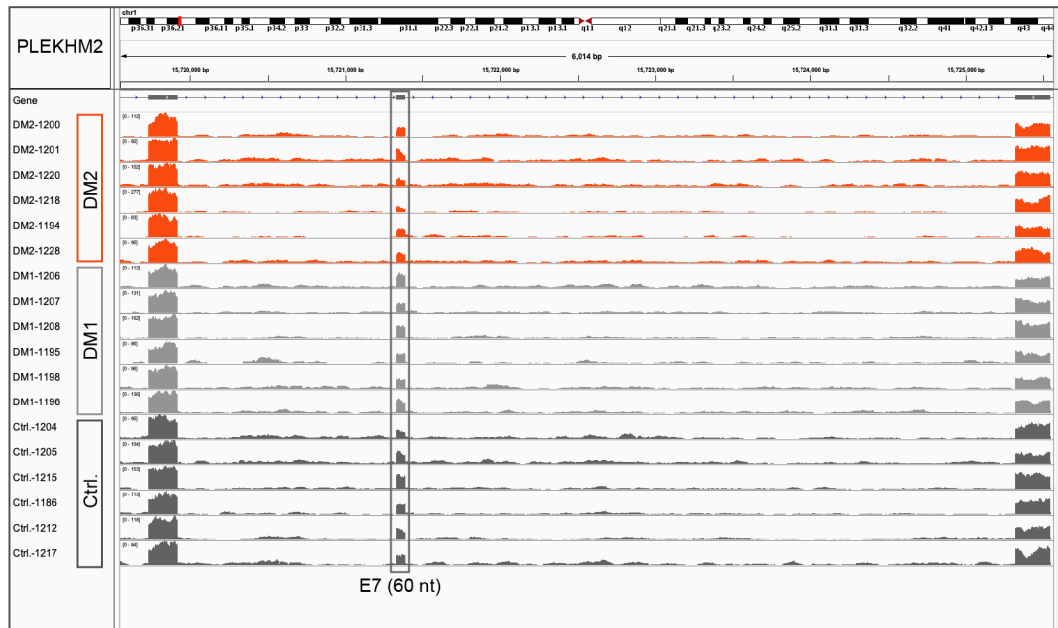


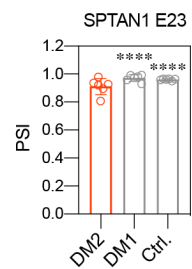
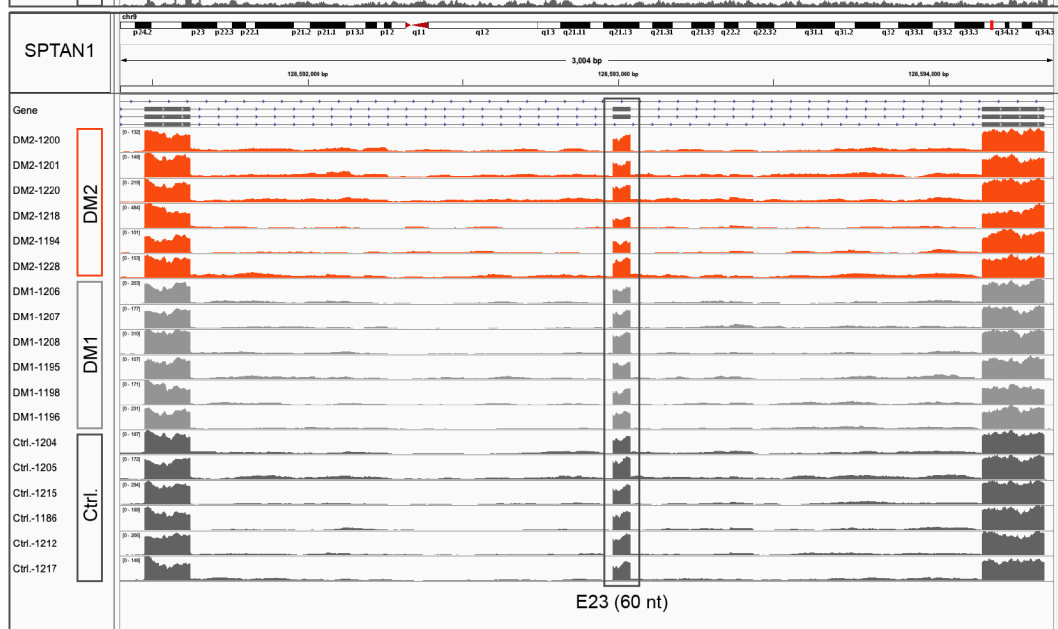
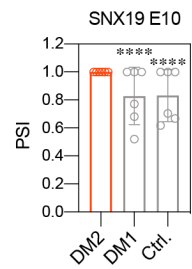
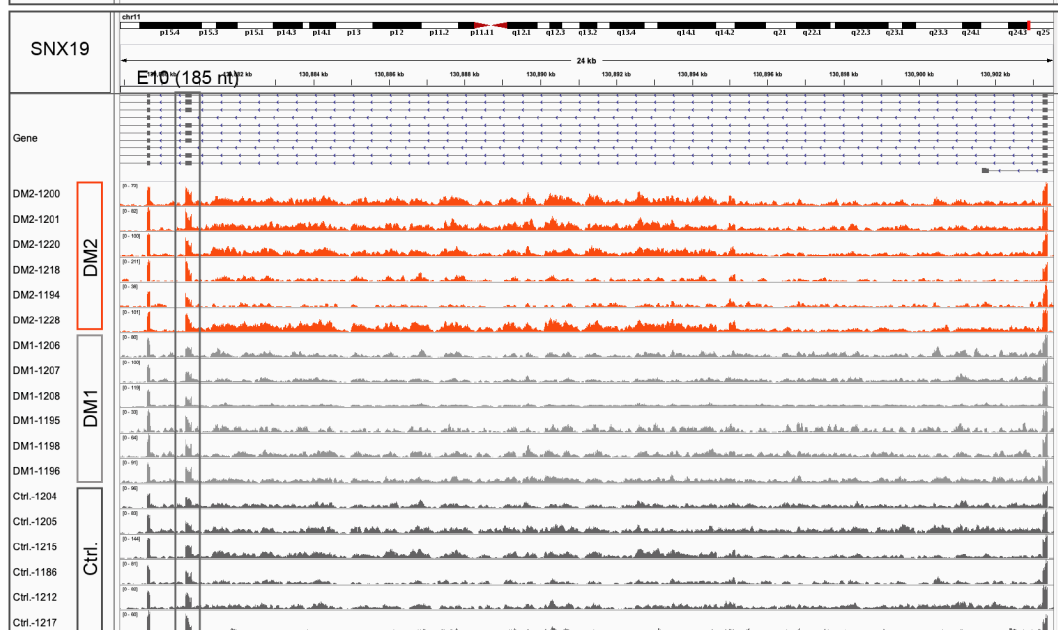
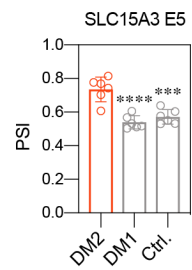
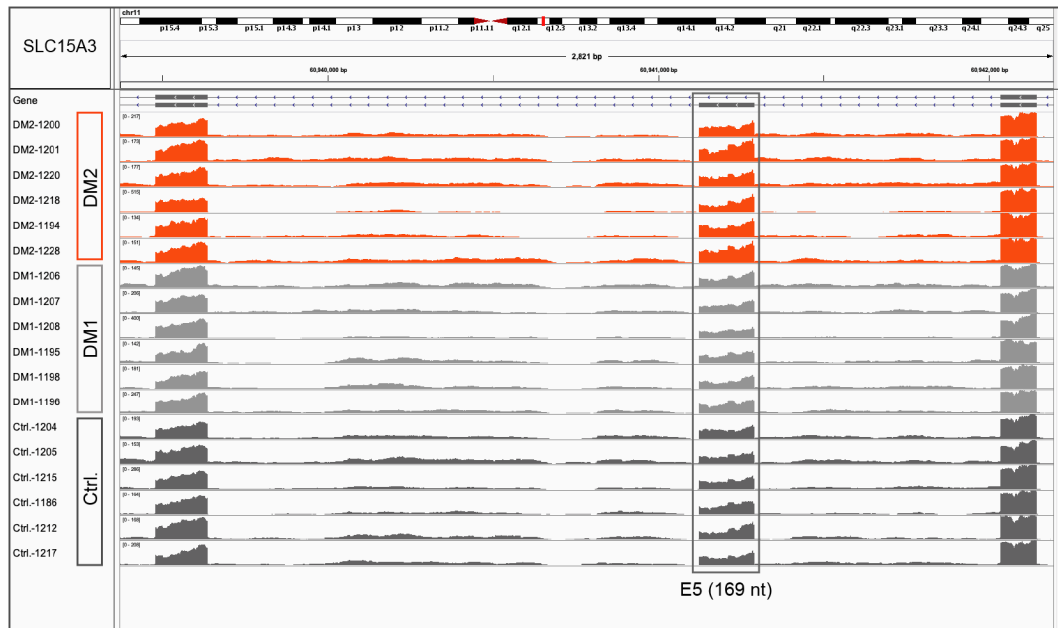




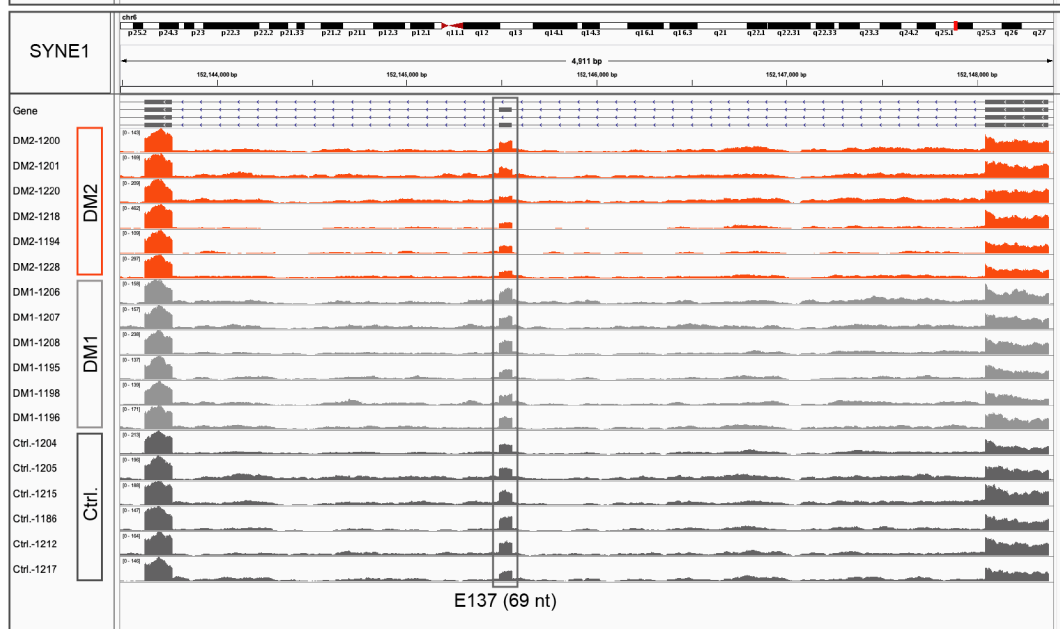
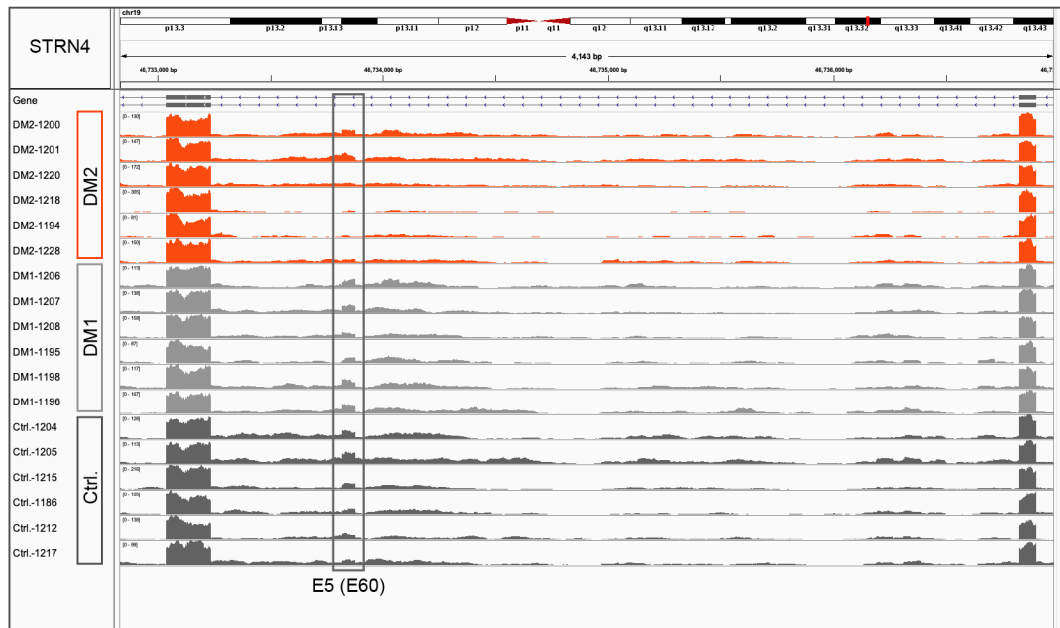


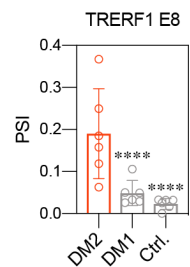
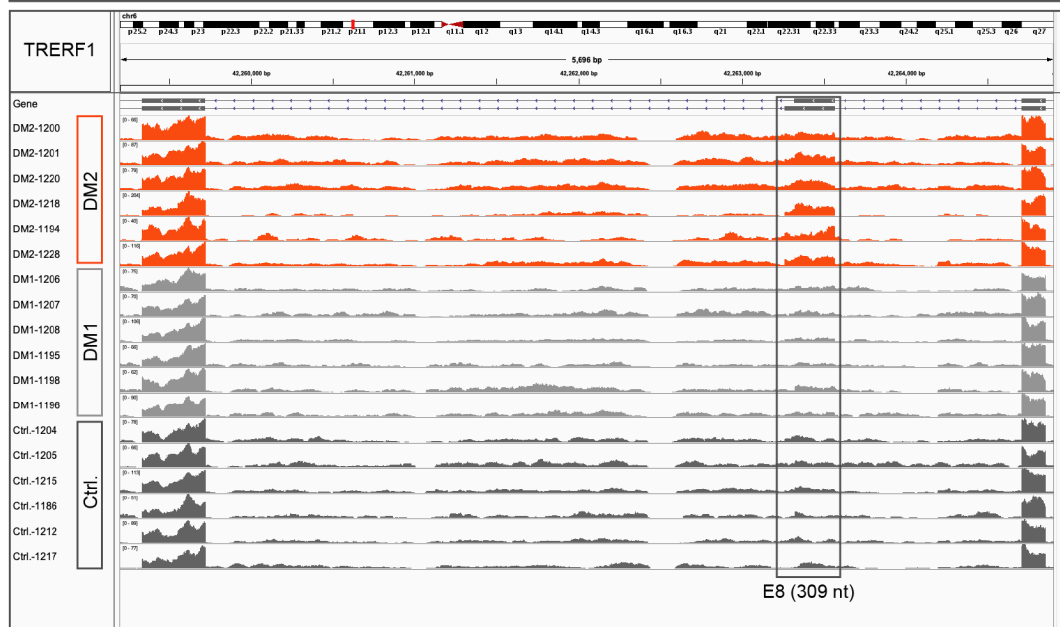
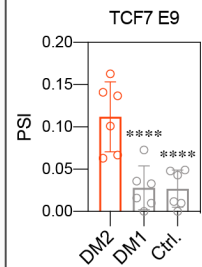
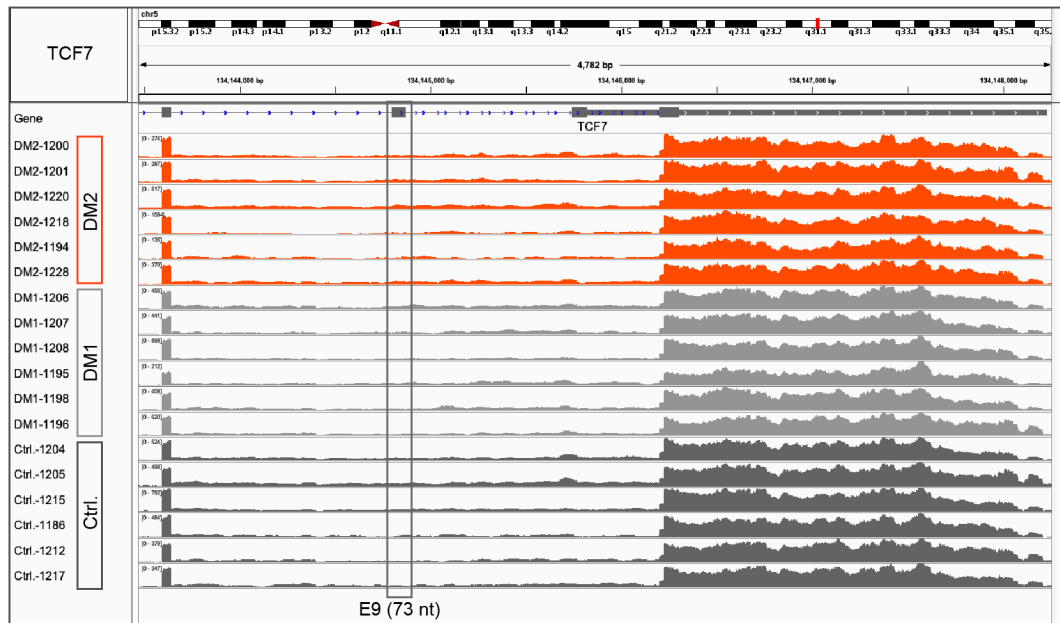
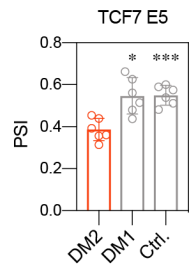
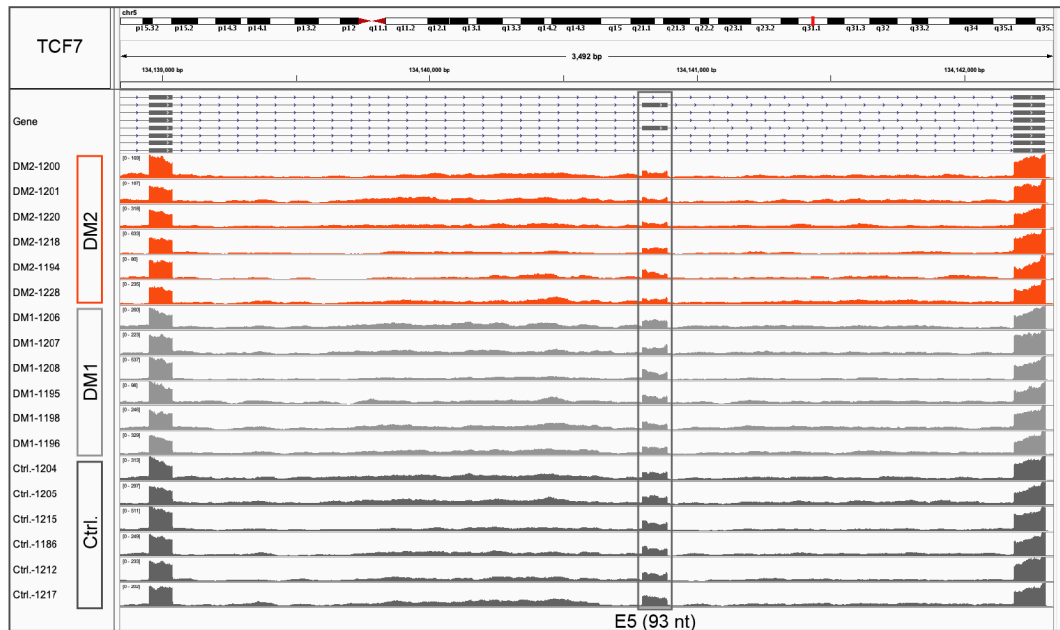


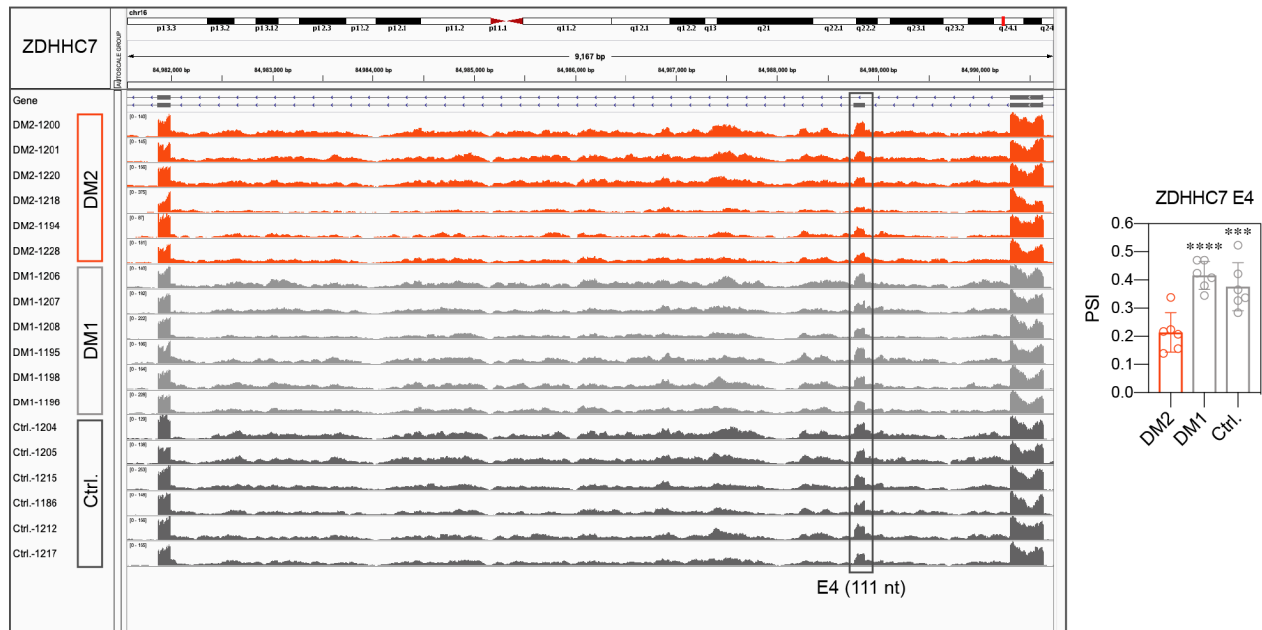








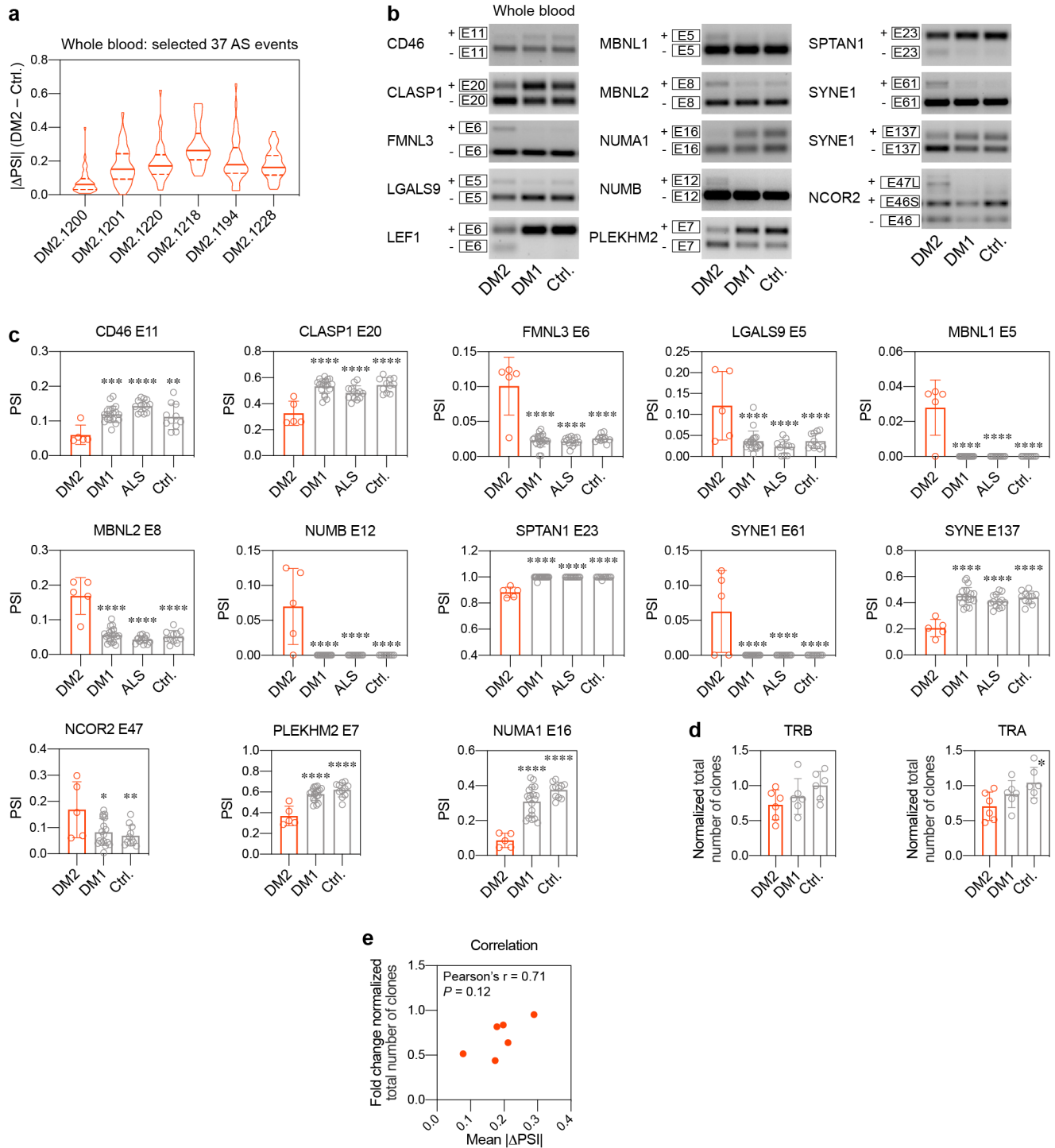




**Supplementary Fig. 8. Genome browser views of selected human alternative splicing events**

Genome browser view of selected AS events from DM2 (n = 6), DM1 (n = 6) and unaffected control (Ctrl.; n = 6) whole blood RNA-seq data. DM2, DM1 and Ctrl. are represented by orange, light grey and dark gray wiggle plots, respectively. Bar graphs show mean PSI ± SD. rMATS; \* FDR < 0.05, \*\* FDR < 0.01, \*\*\* FDR < 0.001, \*\*\*\* FDR < 0.0001.

Source data are provided as a Supplementary Data 1 file.



### Supplementary Fig. 9. Alternative splicing changes in DM2 whole blood

**a** Six DM2 whole blood samples representing different levels of spliceopathy detected. Violin plot represents the distribution of  $|\Delta\text{PSI}|$  values for 37 selected AS events. Center line represents the median, and the dash lines extend from the 25<sup>th</sup> to 75<sup>th</sup> percentiles.

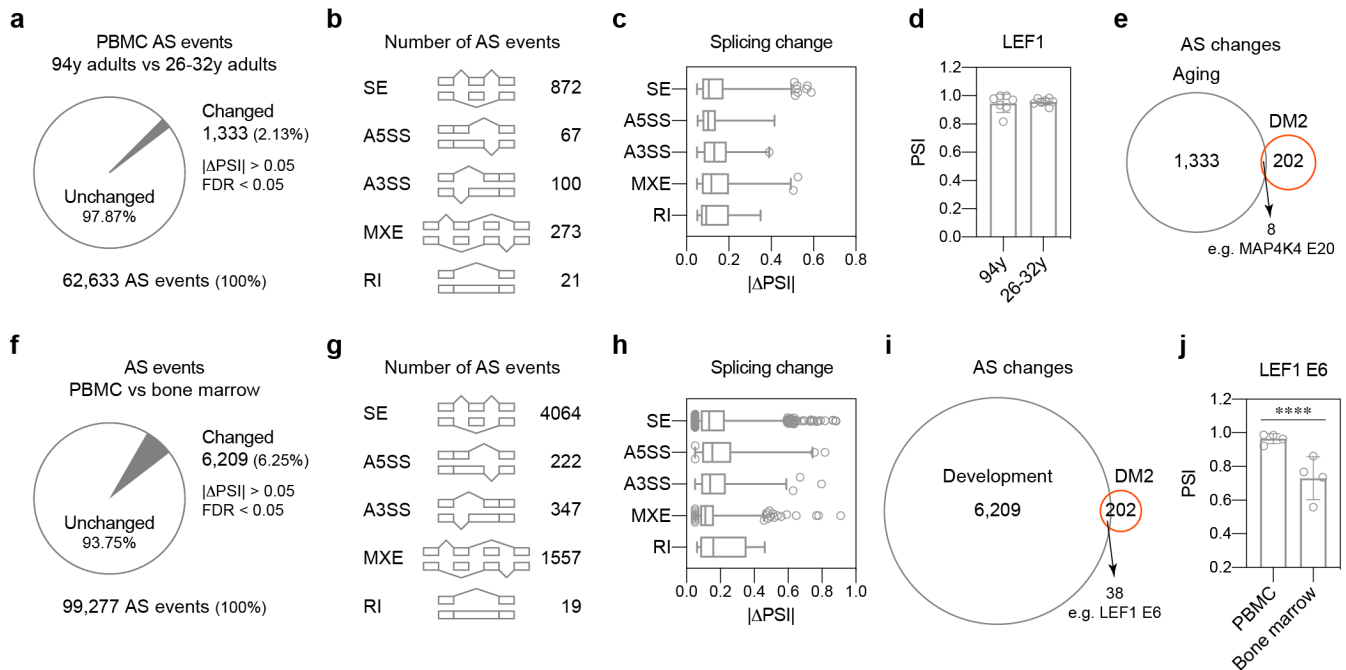
**b** Representative gels of 14 AS event RT-PCR assays on DM2, DM1 and unaffected control (Ctrl.) whole blood samples.

**c** Aberrant AS events in a large cohort of DM2 (n = 5), DM1 (n = 19), ALS = (n = 13) and unaffected (n = 11) control whole blood samples. Bar graphs show mean PSI  $\pm$  SD. Significant difference were determined by Dunnett's multiple comparison test: \*  $P_{adj} < 0.05$ , \*\*  $P_{adj} < 0.01$ , \*\*\*  $P_{adj} < 0.001$ , \*\*\*\*  $P_{adj} < 0.0001$ .

**d** Aberrant TCR repertoire detected in whole blood RNA-seq. Bar graphs show mean total number of clones normalized to uniquely mapped reads  $\pm$  SD. Significant difference were determined by Dunnett's multiple comparison test: \*  $P_{adj} = 0.022$ .

**e** Correlation between fold change TCR repertoire and spliceopathy in DM2 (n = 6) whole blood RNA-seq. TCR repertoire represents fold change normalized total number of TRB and TRA clones. Mean spliceopathy is represented by 37 selected AS events.

Source data are provided as the Source Data and Supplementary Data 1 files.



### Supplementary Fig. 10. Blood DM2 alternative splicing changes are not age dependent

**a** Pie chart represents all detected AS events in the PBMC RNA-seq data. Gray triangle represents significantly changed AS events in PBMC obtained from 94 year-old ( $n = 7$ ) compared to 26-32 year-old females ( $n = 7$ ) - GSE122309<sup>4</sup>.

**b** Number of significantly changed AS events assigned to different categories.

**c** Wide range of splicing changes. Box plot of AS event  $|\Delta\text{PSI}|$  values. Center line represents the median, and the box extends from the 25<sup>th</sup> to 75<sup>th</sup> percentiles. Whiskers show 1-99 percentile.

**d** Aging does not influence LEF1 E6 splicing. Bar graph shows mean  $\text{PSI} \pm \text{SD}$ . rMATS;  $\text{FDR} > 0.05$ .

**e** Venn diagram shows minimal overlap between AS changes during aging (PBMC) and DM2 (whole blood).

**f** Pie chart represents all detected AS events in the PBMC RNA-seq data. Gray triangle represents significantly changed AS events in PBMCs ( $n = 4$ ) compared to bone marrow ( $n = 4$ ) - GSE58335 and GSE61410<sup>3</sup>.

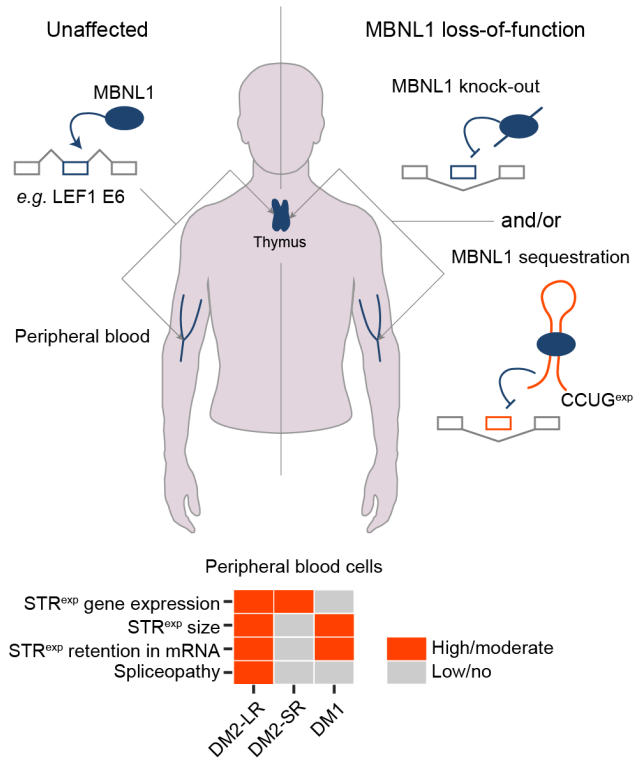
**g** Number of significantly changed AS events assigned to different categories.

**h** Wide range of splicing changes. Box plot of AS event  $|\Delta\text{PSI}|$  values. Center line represents the median, and the box extends from the 25<sup>th</sup> to 75<sup>th</sup> percentiles. Whiskers show 1-99 percentile.

**i** Venn diagram shows overlap between AS changes during blood cell development and DM2 (whole blood).

**j** LEF1 E6 splicing is developmentally regulated. Bar graph shows mean  $\text{PSI} \pm \text{SD}$ . rMATS; \*\*\*\*  $\text{FDR} < 0.0001$ .

Source data are provided as a Supplementary Data 1 file.



### Supplementary Fig. 11. Graphical abstract

MBNL1 depletion leads to pre-mRNA misprocessing in lymphoid organs and cells. A high load of CCUG repeats cause spliceopathy in myotonic dystrophy type 2 peripheral blood cells. STR<sup>exp</sup> - short tandem repeat expansion; LR - long repeats; SR - short repeats.

## Supplementary References

- 1 Kernfeld, E. M. *et al.* A Single-Cell Transcriptomic Atlas of Thymus Organogenesis Resolves Cell Types and Developmental Maturation. *Immunity* **48**, 1258-1270.e1256, doi:10.1016/j.immuni.2018.04.015 (2018).
- 2 Bagger, F. O., Kinalis, S. & Rapin, N. BloodSpot: a database of healthy and malignant haematopoiesis updated with purified and single cell mRNA sequencing profiles. *Nucleic Acids Res* **47**, D881-D885, doi:10.1093/nar/gky1076 (2019).
- 3 Dvinge, H. *et al.* Sample processing obscures cancer-specific alterations in leukemic transcriptomes. *Proc Natl Acad Sci U S A* **111**, 16802-16807, doi:10.1073/pnas.1413374111 (2014).
- 4 Nevalainen, T. *et al.* Aging-associated patterns in the expression of human endogenous retroviruses. *PLoS One* **13**, e0207407, doi:10.1371/journal.pone.0207407 (2018).